MICRO-NANO MECHATRONICS – NEW TRENDS IN MATERIAL, MEASUREMENT, CONTROL, MANUFACTURING AND THEIR APPLICATIONS IN BIOMEDICAL ENGINEERING

Edited by **Toshio Fukuda, Tomohide Niimi** and **Goro Obinata**

INTECHOPEN.COM

Micro-Nano Mechatronics – New Trends in Material, Measurement, Control, Manufacturing and Their Applications in Biomedical Engineering
http://dx.doi.org/10.5772/55984
Edited by Toshio Fukuda, Tomohide Niimi and Goro Obinata

Contributors
Toshio Fukuda, Masahiro Nakajima, Masaru Kojima, Goro Obinata, Hitoshi Hirata, Chikara Nagai, Shigeru Kurimoto, Shuichi Kato, Tomonori Nakano, Tomohide Niimi, Eiji Shamoto, Norikazu Suzuki, Takashi Kato, Burak Sencer, Tomohiro Kawahara, Fumihito Arai, Osamu Takai, Maria Antoaneta Bratescu, Tomonaga Ueno, Nagahiro Saito, Minoru Ueda, Nobutada Ohno, Dai Okumura, Yusuke Kinoshita, Kenji Fukuzawa, Ken-ichi Isobe, Naomi Nishio, Thanasegaran Suganya, Zhao Cheng, Sachiko Ito, Noritsugu Umehara, Takayuki Tokoroyama, Hiroyuki Kousaka, Yang Ju, Akihiro Sasoh, Kensuke Kuroda, Masazumi Okido, Masaru Takeuchi, Gauvain Haulot, Chih-Ming Ho, Daniel T. Kamei, Hideharu Hibi, Mitsuhiro Shikida and Yajing Shen

Published by InTech
Janeza Trdine 9, 51000 Rijeka, Croatia

Publishing Process Manager Danijela Duric
Typesetting www.pantype.com
Cover InTech Design Team

First published March, 2013
Printed in Croatia

A free online edition of this book is available at www.intechopen.com
Additional hard copies can be obtained from orders@intechopen.com

Micro-Nano Mechatronics – New Trends in Material, Measurement, Control, Manufacturing and Their Applications in Biomedical Engineering,
Edited by Toshio Fukuda, Tomohide Niimi and Goro Obinata
p. cm.
ISBN 978-953-51-1104-7

IntechOpen

IntechOpen

Contents

IntechOpen

IntechOpen

Preface

Micro/Nano mechatronics is currently used in broader spectra, ranging from basic applications in robotics, actuators, sensors, semiconductors, automobiles, and machine tools. As a strategic technology highlighting the 21st century, this technology is extended to new applications in bio-medical systems and life science, construction machines, and aerospaceequipment, welfare/human life engineering, and other brand-new scopes. Basically, the miniaturizing technology is important to realize high performance, low energy consumption, low cost performance, small space instrumentation, light-weight, and so on.

In this book, the states of art of research progress are summarized through our project "COE for Education and Research of Micro-Nano Mechatronics" and the R&D in "Center For Micro-Nano Mechatronics" at Nagoya University. Our project strives to foster "young researchers who dare to challenge unexploited fields" by building a novel interdisciplinary field based on micro-nano mechatronics. This field is important to promote "the world-highest-level of micro-nano mechatronics research with an emphasis on originality" from a viewpoint of not only the acquisition of advanced technology, but also social issues.

Our project implements a strategy to realize applications of micro-nano mechatronics, which are based on mechanical engineering or materials science, control systems engineering, and advanced medical engineering. As shown in Figure 1, the proposed research teams include "Nanocontrol engineering", "Nano measurement engineering", "Nano design and manufacturing", and "Nano materials science".

By establishing joint research and international collaborations between the above research teams, we have created the most advanced micro-nano mechatronics. We have also trained the researchers who can comprehend industrial circles and social issues using an open cluster system as well as conduct research to solve problems spanning these four basic fields. In particular, we initially focus on tasks in the bio- or medical welfare technologies using a number of unexploited fields, which may consequently produce venture enterprises.

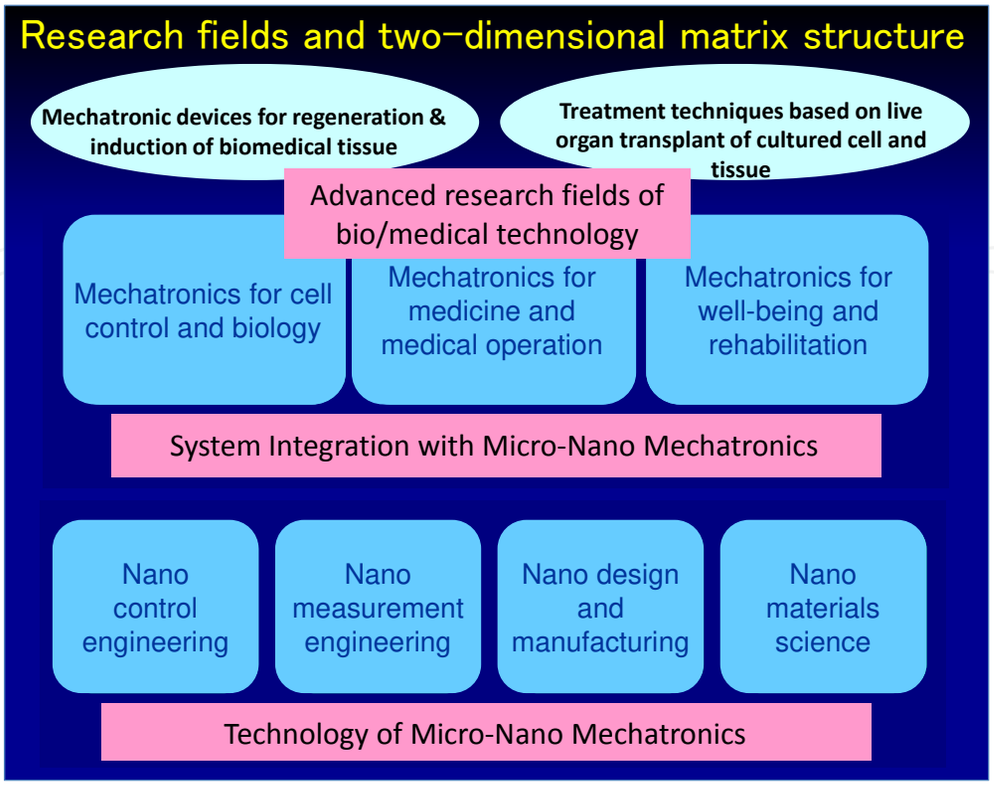

Figure 1. Innovations by micro-nano mechatronics.

We acknowledge the excellent contributions of all people to contribute the chapters for this book. We express our sincere appreciation for the publication of this book supported by Nagoya University, the 21st COE program "Micro- and Nano-Mechatronics for Information-Based Society", and the global COE program “COE for Education and Research of Micro-Nano Mechatronics”. This book would not have been possible without these generous supports.

Nagoya, December 2012

Toshio Fukuda
Graduate School of Engineering, Nagoya University
Japan

IntechOpen

IntechOpen

Chapter 1

Research and Technology on Micro-Nano Mechatronics

Toshio Fukuda, Masahiro Nakajima and
Masaru Kojima

1. Introduction

In our daily life, various devices are applied for automobiles, computer peripheries, printers, cameras, amusements, robotics, automation, environmental monitoring, energy resource, biological/medical treatments, and so on "Microtechnology" was commonly used to realize high-efficiency, high-integration, high-functionality, low-energy consumption, low-cost, miniature, and so on By miniaturizing the elemental devices on sensors, actuators, and computers in micro-scale, "Micromechatronics" came up as the one of the important technology Recently, "Nanotechnology" has an important role in the industrial applications as an advanced field of mechatronics named as "Nanomechatronics" The micro-nano mechatronics is basically defined to integrate major three technologies "Controller", "Sensor" and "Actuator" based on the electronics and mechanical engineering as depicted in Figure 1.

Figure 2 shows the demands of micro-nano mechatronics for various social and industrial applications For various applications for industry, some techniques are important, especially micro/nano fabrication, assembly, control, material, and evaluation techniques Micro-nano mechatronics is based on various technologies, especially life science, medicine, sensing/actuating, material science, energy/power, and design/control From social aspects, human resource, environmental issue, saving energy, safety/security, medical/health, and aging population are currently demanded From industrial aspects, service robots, dependable products, tailor-made products, alternative energy, techno-care service, environmental friendly products, are particularly demanded The micro-nano mechatronics is a key technology to solve those problems/issues and leading conventional technologies for future.

The applications of micro-nano mechatronics are mainly categorized into the "Mechanical", "Electrical", and "Biological/Medical" applications The key point for the categorization is inorganic (wet) and organic (dry) "Mechanical" applications are relatively based on the inorganic materials or technologies, such as lithography technique On the other hand, "Biological/Medical" applications, the organic materials or technologies are used, such as self-

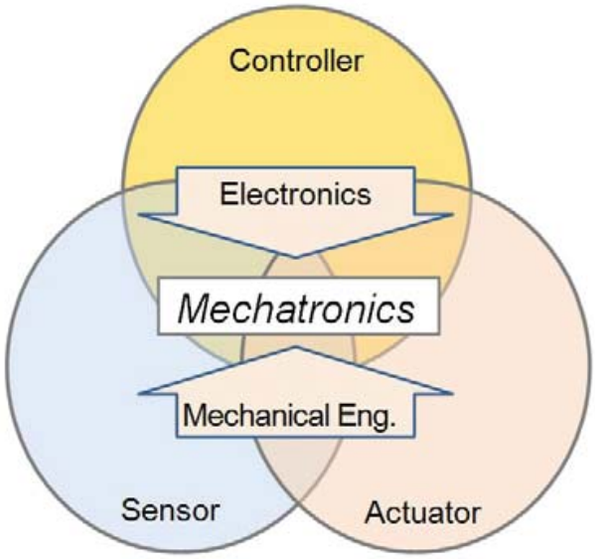

Figure 1. Micro-Nano mechatronics

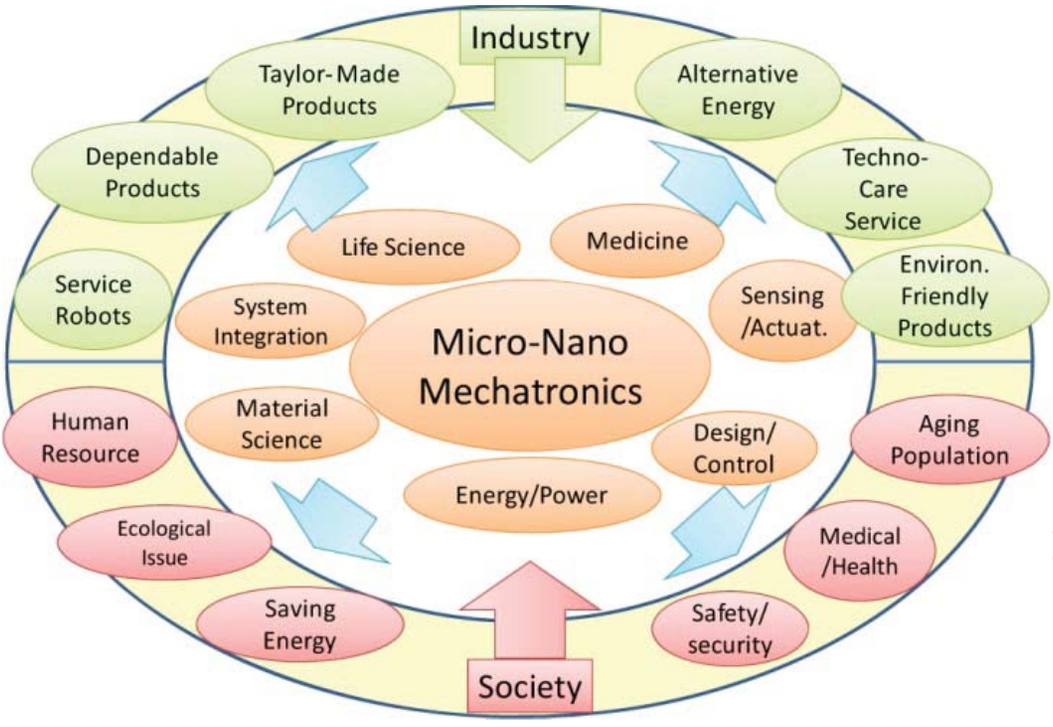

Figure 2. Micro-Nano mechatronics for social and industrial demands

assembly technique In between them, "Electrical" applications are placed for delivering or calculating information and so on Since the micro-nano mechatronics is the composite academic fields, the required technologies are mainly categorized in to basic/middle/high integration levels as depicted in Figure 3.

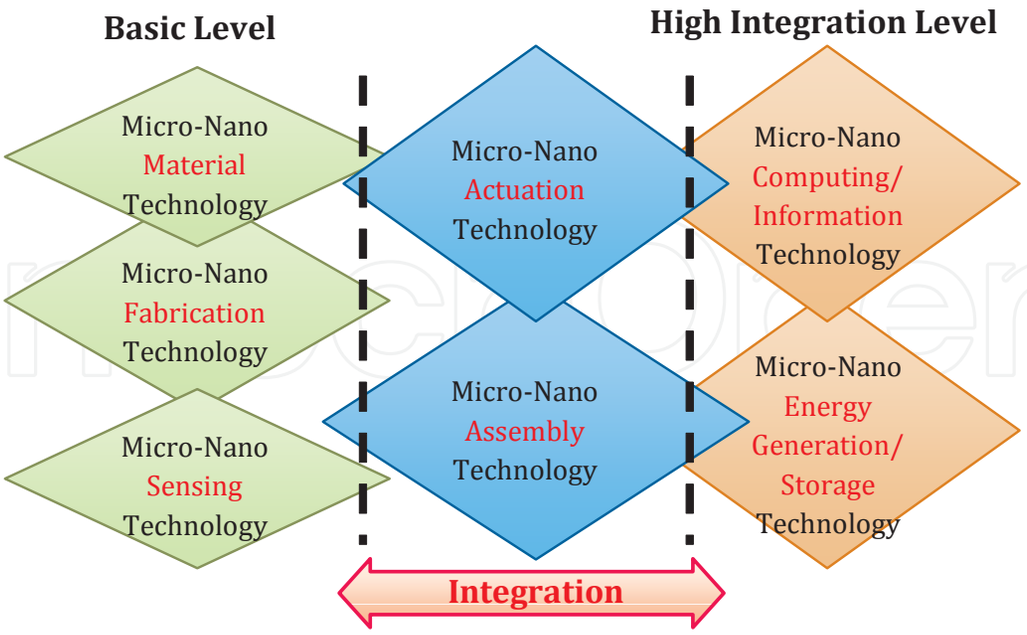

Figure 3. Required technologies for micro-nano mechatronics

Basically, nanotechnology is placed in the combinations of the top-down and bottom-up approaches The possibility to control the structure of matter atom by atom was first discussed by Richard Feynman in 1959 seriously [1] One of the approaches to fill the gap between top-down and bottom-up approaches is "Nanomanipulation", which realizes controlling the position at the micro/nanometer scale, is considered to be one of the promising ways It might be a key technology to lead the appearance of replication-based assemblers The top-down fabrication process, or micro machining, provides numbers of nanometer structures at once On the other hand, the bottom-up fabrication process, or chemical synthesis such as self-assembly [2] , also provides numerous nanometer structures In fact, both approaches reach nanometer scale with the limitations of physical/chemical aspects at present Hence, the technology to fill its gap is considered to be one of the important at this moment for micro-nano mechatronics Especially, current research directions are mainly two flows, "green innovation" and "life innovation" as depicted in Figure 4 These innovations will be achieved in various research and developments Table 1 and 2 show the challenging issues by categorized fields.

2. Micromechatronics for industrial and research applications

In micro scale, the important technologies are Micro Machine, Micro Mechatronics, Micro Fabrication and Assembly for micromechatronics Recently, borderless applications are investigated such as Micro Biology, Wet Mechatronics, Micro Total Analysis System, Micro Medical Engineering, and Regenerative Medical Engineering Some examples of micro devices mainly in research field are micro-actuator [3] , micro-ink-jet head [4] , micro-force sensor [5] , micro-tactile sensor [6] , micro-fuel battery[7] , micro fluidics device[8] , blood vessel simulator [9] , and so on.

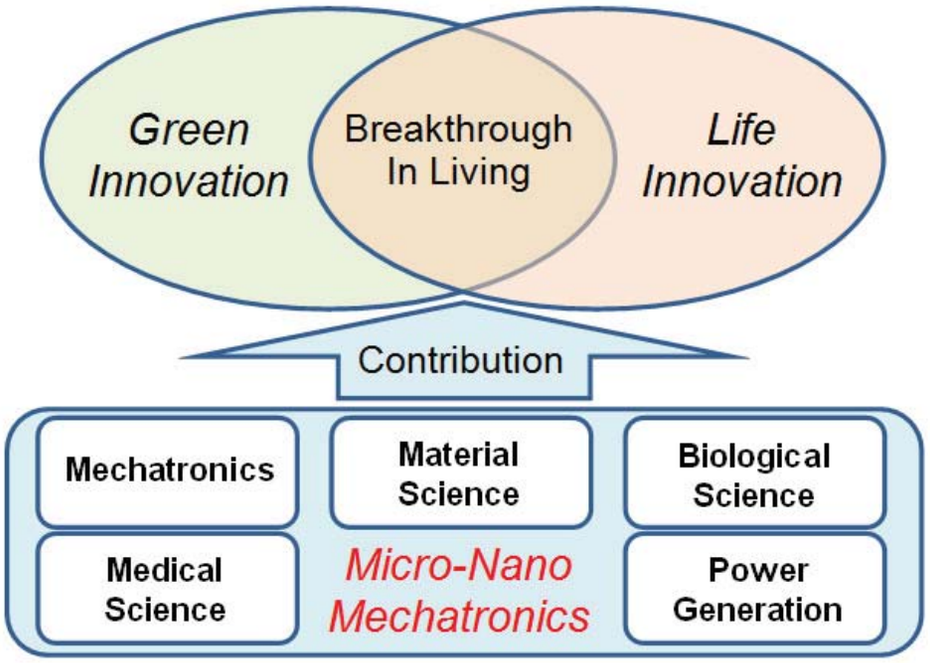

Figure 4. Green and life innovations based on micro-nano mechatronics

Green innovation	Technological Challenges
Natural Resources	Micro/nano devices for Discovery of oil resource, Management of water resources, Prevention of forest destruction, etc
Environmental Pollution	Monitor, control and management of Environment, Distributed sensing & control, Pollution control, Green vehicle, etc
Energy Development	Energy saving, harvesting and alternatives , Energy grid and management, Power control and green electronics, etc
Food and Agriculture	Safety, testing and tracing, Efficient harvesting, nutritious products, genetically-modified products, etc

Table 1. Challenges for green innovation by micro-nano mechatronics

Life innovation	TechnologicalChallenges
Medicine for life	Inspection and diagnosis , Re-generative medicine, Gene therapy and life science, monitoring diseases, Neuro Science, In-situ diagnostics, Cell diagnosis and surgery, New drug and medicine, DDS, Minimally invasive surgery, Rehabilitation, Techno-care, Wearable robots, Cyborg, QoL, etc
Biology–Analysis and Synthesis	Sensing , manipulation and automation, New species, DNA diagnosis & manipulation, Cell screening, transport, cultivation, and function and differentiation control, Artificial cell, Life in chip, Cloning of stem cells, etc

Table 2. Challenges for life innovation by micro-nano mechatronics

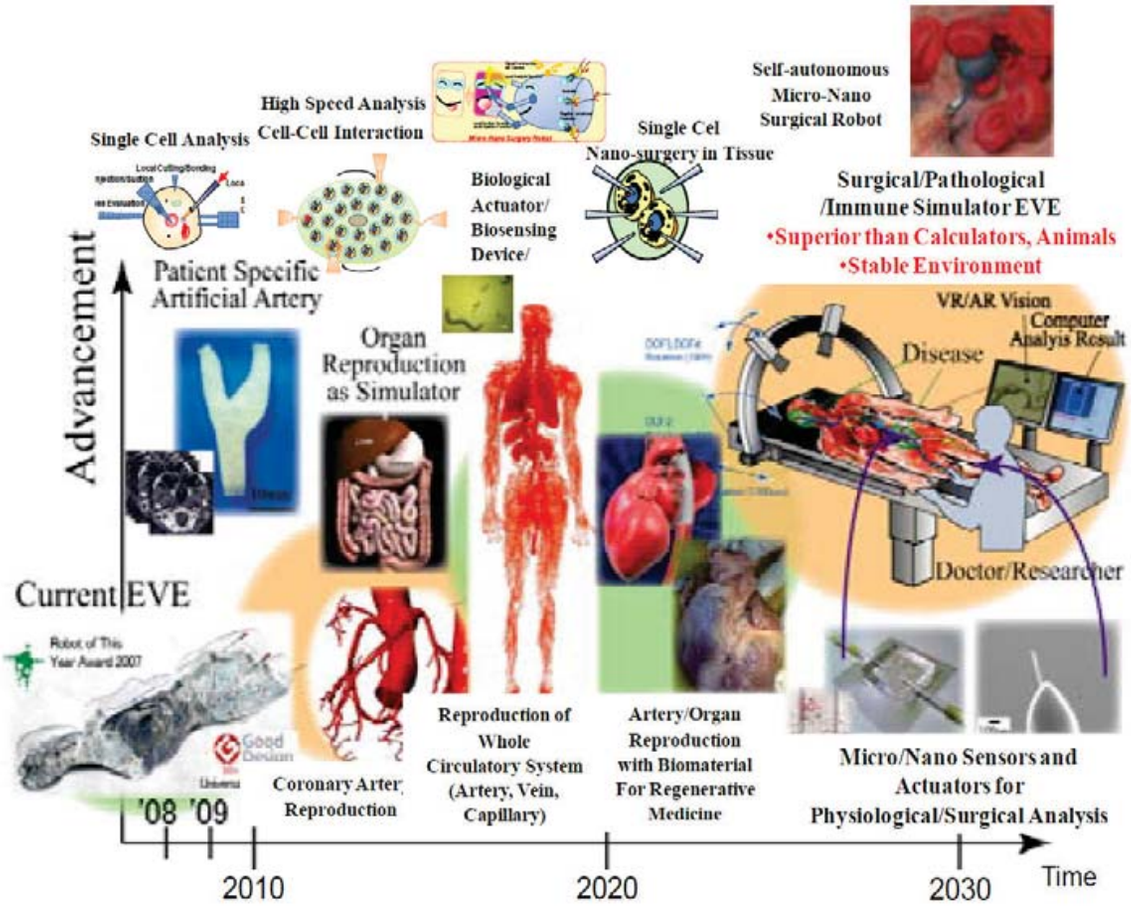

Figure 5. Blood vessel simulator and surgical operation system

In medical applications, surgical supporting or simulating technologies are important We developed the Patient blood vessel simulator "EVE (Endo Vascular Educator)" as challenging the frontier of the surgical simulation since 1989 This simulator is fabricated and assembled based on the micro-fabrication technologies of rapid prototyping technique [9] .

Recently, we have interests to realize the "In vitro" realization of "In vivo" environment For the purpose, it is needed to understand our biological system in detail The investigation approach using micro/nano devices can measure and control inside "In vivo" biological system Moreover, "In vitro" constructions and measurements of biological system can reveal it clearly in single/multiple cell It is quite important for the significant improvement of regeneration engineering/biology, inducing the evaluation of clinical condition of blood vessel We have been worked blood vessel simulator and surgical operation system to improve and integrate for the "In vivo" realization Based on the EVE system, we are trying to develop novel type of surgical simulation system with the "In vitro" realization of "In vivo" environment The human cells can be used to construct as blood vessel or other organs including diseases by 3D cell assembly technique The surgical simulator can be integrated with micro-nano sensors and

devices to evaluate the surgical operations and other applications such as drug delivery system.

3. Nanomechatronics for industrial and research application

In nano scale, the important technologies are Nano-measurement, Nano-fabrication and Nano-assembly for nanomechatronics The advanced applications are investigated for quantum dots [10] , quantum processing [11] , photonic crystal [12] , drug delivery system (DDS) [13] , field emission display [14] , nano-field emission electron source [15] , nano-X-ray sources [16] , nano-actuator[17] , nano-temperature sensor[18] , nano-IR sensor[19] , super-molecules for solar energy conversion [20] , and so on.

The wide scale controlled devices from atomic scale to meter scale is expected to realize in the near future For the high integrated, miniaturized, and functionalized NEMS, one of the effective ways is to use the bottom-up fabricated nanostructures or nanomaterials directly As typical example, the nanodevices are investigated based on the carbon nanotubes (CNTs) It has interesting mechanical, electronic and chemical properties which have been under investigation in various studies [21] There is possibility to use their fine structures directly For example, “telescoping carbon nanotube”, which is fabricated by peeling off the outer layers of multi-walled carbon nanotubes (MWNTs), is one of the most interest nanostructures As previous works, the pulling out of the inner core was pulled out mechanically inside a TEM [22] The MWNTs were used them as the rotation axis of silicon chip as rotational actuators [23] .We reported on the direct measurements of electrostatic actuation of a telescoping MWNT inside SEM and TEM [17] [24] [25] Those applications are newly developed using the bottom-up structures of CNTs.

4. Research on center for micro-nano mechatronics in Graduate School of Engineering, Nagoya University

We established a "Center for Micro-nano Mechatronics" at Graduate School of Engineering, Nagoya University in 2008 with the aim of applying nanotechnology to practical systems in micro-nano scale from a system approach viewpoint [26] Our Center strives to foster “young researchers who dare to challenge unexploited fields” by building a novel interdisciplinary field based on micro-nano mechatronics This field will promote “the world-highest-level of micro-nano mechatronics research with an emphasis on originality” from a viewpoint of not only the acquisition of advanced technology, but also social issues.

Our center aims not only to create novel functional materials and advanced mechatronics, but also to discover breakthroughs in next-generation medicine we promote researches in four

basic fields, Nano control engineering, Nano measurement engineering, Nano design and manufacturing, and Nano materials science and conduct an applied research encompassing all these basic research fields to attend to the needs of the advanced medical engineering.

Our center implements a strategy to realize applications of micro-nano mechatronics, which are based on mechanical engineering or materials science, control systems engineering, and advanced medical engineering As shown in Figure 6, by establishing joint research and international collaborations between the above research fields, we are creating the most advanced micro-nano mechatronics and train researchers who can comprehend industrial circles and social issues using an open cluster system as well as conduct research to solve problems spanning these four basic fields In particular, we will initially focus on tasks in the bio- or medical welfare technologies using a number of unexploited fields, which may consequently produce venture enterprises Some research results are figured as shown in Figure 7 in the four basic research fields Detail information or more recent results will be given by the following chapters in this book.

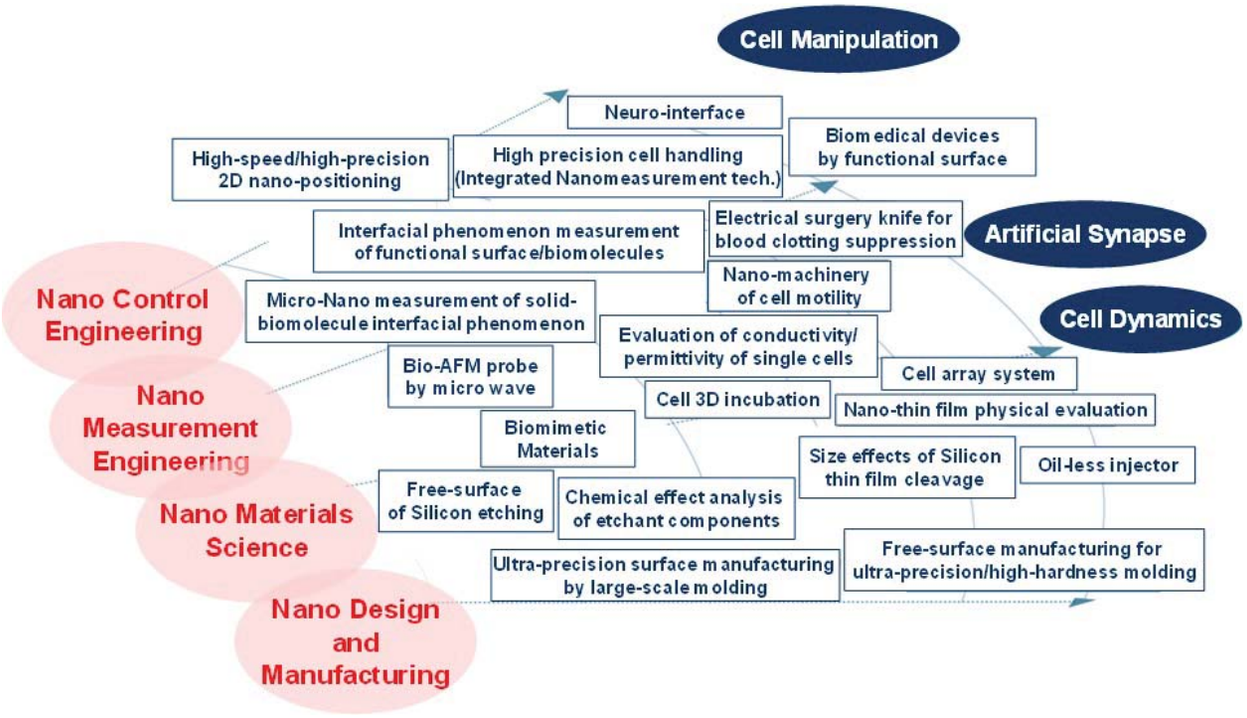

Figure 6. Milestone of Micro-Nano mechatronics research fields

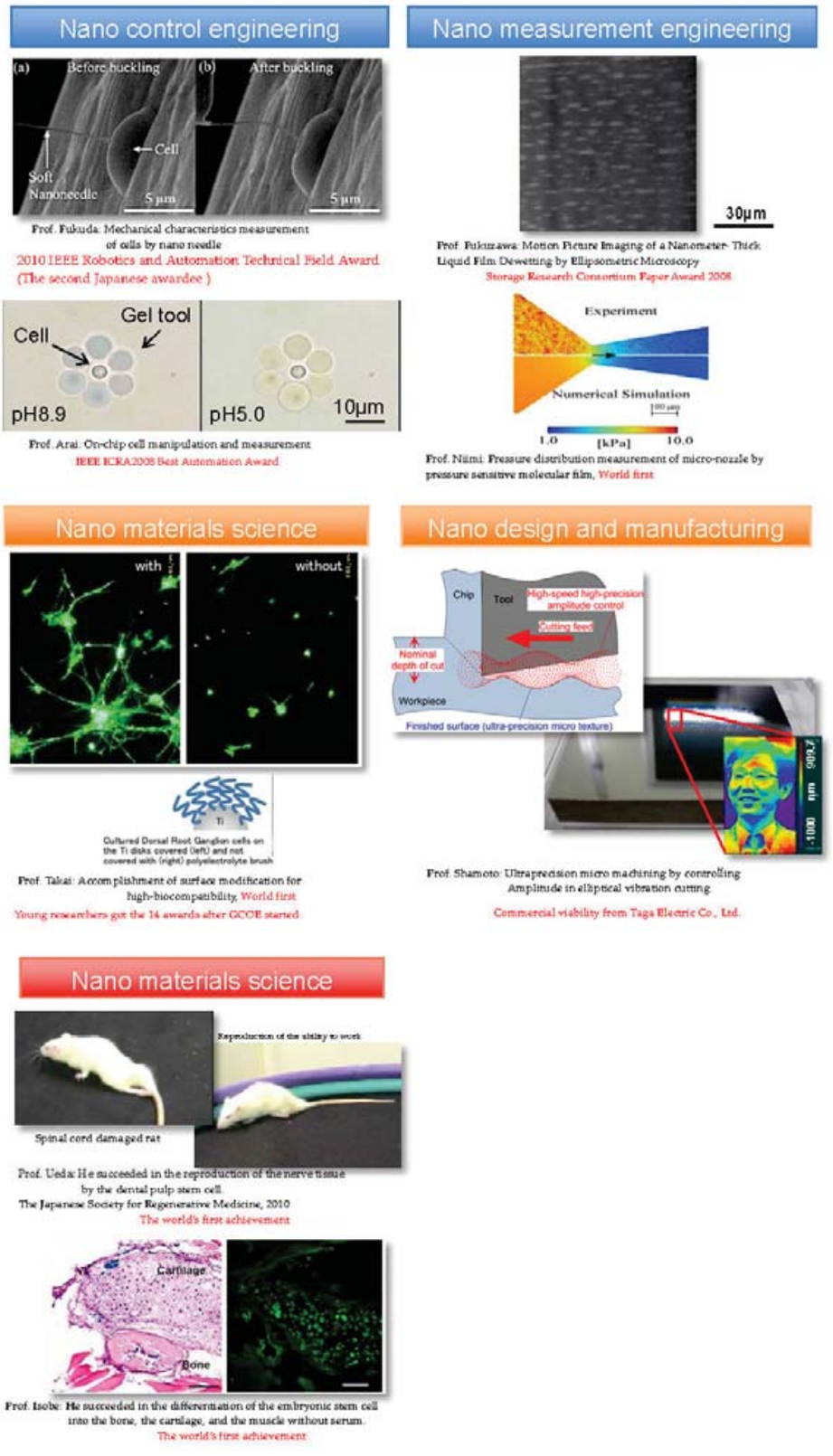

Figure 7. Examples of research results of micro-nano mechatronics from the center for micro-nano mechatronics of Nagoya University

5. Conclusion

This chapter presents the brief introduction of research and technology on micro-nano mechatronics For industrial applications, various devices are developed and available, such as applications to the automobiles, computer peripheries, amusements, printers, cameras, robotics automation, environmental monitoring, biological/medical treatments, energy resource, and so on Those devices are investigated based on the micro-and nano-mechatronics technologies to realize high-efficiency, high-integration, high-functionality, low-energy consumption, low-cost, miniature, and so on Micro-nano mechatronics technologies can be applied to break though the advanced industrial field including the nanobiology and medical applications.

Author details

Toshio Fukuda[1], Masahiro Nakajima[2] and Masaru Kojima[1]

1 Department of Micro-Nano Systems Engineering, Nagoya University, Nagoya, Japan

2 Graduate School of Engineering Center For Micro-nano Mechatronics, Nagoya University, Nagoya, Japan

References

[1] Feynman R. P. There's Plenty of Room at the Bottom. Caltech's Engineering and Science 1960;23 22-36.

[2] Whitesides G. M, Grzybowski B. Self-Assembly at All Scales. Science 2002;295 2407-2409.

[3] Kanno I, Tazawa Y, Suzuki T, Kotera H. Piezoelectric unimorph miroactuators with X-shaped structure composed of PZT thin film. Microsystem Technologies 2007;13(8) 825-829.

[4] Ishida Y, Hakiai K, Baba A, Asano T. Electrostatic Inkjet Patterning Using Si Needle Prepared by Anodization. Japanese Journal of Applied Physics 2005;44(7B) 5786-5790.

[5] Sun Y, Nelson B. J. MEMS Capacitive Force Sensors for Cellular and Flight Biomechanics. Biomedical Materials 2007;2(1) 16-22.

[6] Motoo K, Arai F, Fukuda T, Katsuragi T, Itoigawa K. High sensitive touch sensor with piezoelectric thin film for pipetting works under microscope. Sensors and Actuators A 2006;126 1-6.

[7] Yoshida K, Hagihara Y, Tanaka S, Esashi M. Normally-closed Electrostatic Micro Valve with Pressure Balance Mechanism for Portable Fuel Cell Application. In: proceedings of 19th IEEE International Conference on Micro Electro Mechanical Systems, MEMS2006, 22-26 January 2006, Istanbul, Turkey.

[8] Motoo K, Toda N, Arai F, Fukuda T, Sekiyama K, Nakajima M. Generation of Concentration Gradient from Two-Layered Flow with High-Speed Switching Microvalve. Biomedical Microdevices 2008;10 329-335.

[9] Ikeda S, Arai F, Fukuda T, Negoro M. An In Vitro Soft Membranous Model of Individual Human Cerebral Artery Reproduced with Visco-Elastic Behavior. In: proceedings of the 2004 IEEE International Conference on Robotics and Automation, ICRA2004, 18-22 April 2005, Barcelona, Spain.

[10] Invitrogen Corporation. http://www.invitrogen.com/ (accessed 26 July 2012).

[11] Niskanen A. O, Harrabi K, Yoshihara F, Nakamura Y, Lloyd S, Tsai J. S. Quantum Coherent Tunable Coupling of Superconducting Qubits. Science 2007;316 723-726.

[12] Vlasov Y. A, O'Boyle M, Hamann H. F, McNab S. J. Active control of slow light with photonic crystal waveguides. Nature 2005;438 65-69.

[13] Kakudo T. S, Futaki S. Transferrin-modified liposomes equipped with a pH sensitive fusogenic peptide: an artificial viral like delivery system. Biochemistry 2004;43(19) 5618-5628.

[14] Saito Y, Uemura S. Field Emission from Carbon Nanotues and its Application to Electron Sources. Carbon 2000;38 169-182.

[15] Yabushita R, Hata K, Sato H, Saito Y. Development of compact field emission scanning electron microscope equipped with multiwalled carbon nanotube bundle cathode. Journal of Vacuum Science and Technology B 2007;25 640-642.

[16] Zhang J, Cheng Y, Lee Y. Z, Gao B, Qiu Q, Lin W. L., Lalush D., Lu J. P., Zhou O. A nanotube-based field emission x-ray source for microcomputed tomography. Review of Scientific Instruments 2005;76 094301.

[17] Nakajima M, Arai S, Saito Y, Arai F, Fukuda T. Nanoactuation of Telescoping Multiwalled Carbon Nanotubes inside Transmission Electron Microscope. Japanese Journal of Applied Physics 2007;42 L1035-1038.

[18] Elshimy H. M, Nakajima M, Imaizumi Y, Arai F, Fukuda T. Fabrication of FIB-CVD Nano Temperature Sensors for Local Temperature Sensing in Water Environments. Journal of Robotics and Mechatronics 2007;19(5) 512-518.

[19] Lee J. U. Photovoltaic effect in ideal carbon nanotube diodes. Applied Physics. Letters 2005;87 073101.

[20] Mandalia H. C, Jain V. K, Pattanaik B. N. Application of Super-molecules in Solar Energy Conversion- A Review. Research Journal of Chemical Sciences 2012;2 89-102.

[21] Iijima S. Helical Microtubules of Graphitic Carbon. Nature 1991;354 56-58.

[22] Cumings J, Zettl A. Low-Friction Nanoscale Linear Bearing Realized from Multiwall Carbon Nanotubes. Science 2000;289 602-604.

[23] Fennimore A. M, Yuzvinssky T. D, Han W. Q, Fuhrer M. S, Cummings J, Zettl A. Rotational Actuators Based on Carbon Nanotubes. Nature 2003;424 408-410.

[24] Dong L. X, Nelson B. J, Arai F, Fukuda T. Towards Nanotube Linear Servomotors. IEEE Transaction on Automation Science and Engineering 2006; 3 228-235.

[25] Nakajima M, Arai F, Fukuda T. In situ Measurement of Young's Modulus of Carbon Nanotube inside TEM through Hybrid Nanorobotic Manipulation System. IEEE Transaction on Nanotechnology 2006;5 243-248.

[26] Center for Micro-nano Mechatronics, Graduate School of Engineering, Nagoya University. http://www.mech.nagoya-u.ac.jp/cmm/index_e.html (accessed 26 July 2012)

IntechOpen

Chapter 2

Neural Interfaces: Bilateral Communication Between Peripheral Nerves and Electrical Control Devices

Goro Obinata, Hitoshi Hirata, Chikara Nagai, Shigeru Kurimoto, Shuichi Kato and Tomonori Nakano

1. Introduction

Neural Interfaces are data links between human nervous system and an external device, and allow the transmission of information to and from the human nervous system to the external device. Bioelectric signals can be obtained from the nervous system, and/or transmitted to the nervous system via implanted or surface electrodes. One beneficial application of such neural interfaces is to obtain control signals from undamaged sensory-motor areas of patient's brain for controlling neuroprosthetic devices such as artificial limbs or wheelchairs. Paralyzed or amputated people can reconstruct certain motor functions by using such neuroprosthetic devices. Brain-machine interfaces, which are direct data links between human brain and machines, are one kind of neural interfaces [1]. Such interfaces have been proposed during this decade to control prosthetic limbs, or to control machines such as wheelchairs or robotic manipulators [2]. However, our present knowledge on brain functions is so limited that we do not fully understand the coding of information expressing the behavior in motions; specially, we do not know the variation of the coding in individual differences or in related thoughts or emotions.

In order to design practical neuroprosthetic devices, we focus on neural interfaces which link peripheral nervous system and external devices in this paper (PNI, Peripheral Neural Interface). Since peripheral nervous system is much simpler than central nervous system, we may avoid the difficult problems which come from our limited knowledge on brain functions while the neuroprosthetic devices interact just with the peripheral nerves. In Section 2, we describe interfaces to peripheral motor neurons by using reinnervation type electrodes. The electrodes are constructed by implanting embryonic neurons into peripheral motor units. The endplates of the implanted neurons which grow into muscles make biological interfaces for motor

commands to the muscles. The other ends of the implanted neurons are connected by special types of electrodes to communicate with electric devices of motor controllers. The diameter of mammalian motor neurons is from 0.5 μm to 20 μm. There is a reason why our research requires bio-compatible micro-nano technologies for achieving such interfaces of new reinnervation type electrodes.

Neuroprosthetic devices with interfaces detecting electromyogram (EMG) are in practical use [3]. Such EMG interfaces require to place the electrodes at the end plate of a motor neuron; thus, the paralyzed or amputated users can not control the paralyzed or amputated muscles with the same passes of motor neurons as before paralyzed or amputated. Moreover, EMG interfaces pickup the signals at end plate of a motor neuron; sensory signals from receptors are not obtainable via EMG. This means that two-way communication by EMG interfaces is impossible. We can assemble sensors and stimulators into a neuroprosthetic device. If we have a way to send the signals from the assembled stimulators to sensory nervous system, ideal neuroprosthetic devices with two-way communication will be achievable. The combination of EMG pickup and electrical stimulation with surface electrodes was proposed for two-way communication [4]. However, there is no clear result on the amount of transmissive information through the afferent passes. In Section 3, we show a preliminary study on the possibility of sensory feedback via axial fibers of peripheral sensory neurons. In other words, we try to achieve an artificial afferent pass for feeding signals back to the brain. A method for improving on the amount of transmissive information has been proposed by using a configuration with multi-channel electrodes.

One application of PNIs is to achieve unconscious muscular movements such as walking, writing, dancing, playing musical instruments, and so on. For an example, in walking motions some neural networks generate the pattern of walking, and the steady behavior is closed within the peripheral nervous system and the pattern generators in spinal cord. The upper central nervous system provides the triggers of walking such as start/stop, speedup/slowdown, turn-right/turn-left. The understanding on pattern generators for walking is now enough to simulate human walking or some animals' walking. In Section 4, we give a walking simulation of "rat" to show the possibility of practical usages of PNIs.

2. Transplantation of embryonic neurons into peripheral nerve forms functional motor units

2.1. Background and purpose

There has been a rapid surge in clinical trials involving stem cell therapies over the last three to four years [5]. Those trials are establishing the clinical pathways for regenerative medicine, especially in nervous system. Since derivation of human embryonic stem cells (hESCs) in 1998 [6], hESCs have been thought a promising source of replacement cells for regenerative medicine. Although Geron Corporation has been no longer enrolling patients for the trial, they conducted the first clinical trial in the United States to evaluate the safety of oligodendrocyte

deformation modes decrease energy gaps, $E_g = E_{CBM} - E_{VBM}$, of SWBNNTs, but torsion has less of an effect on the energy gap than tension and flattening.

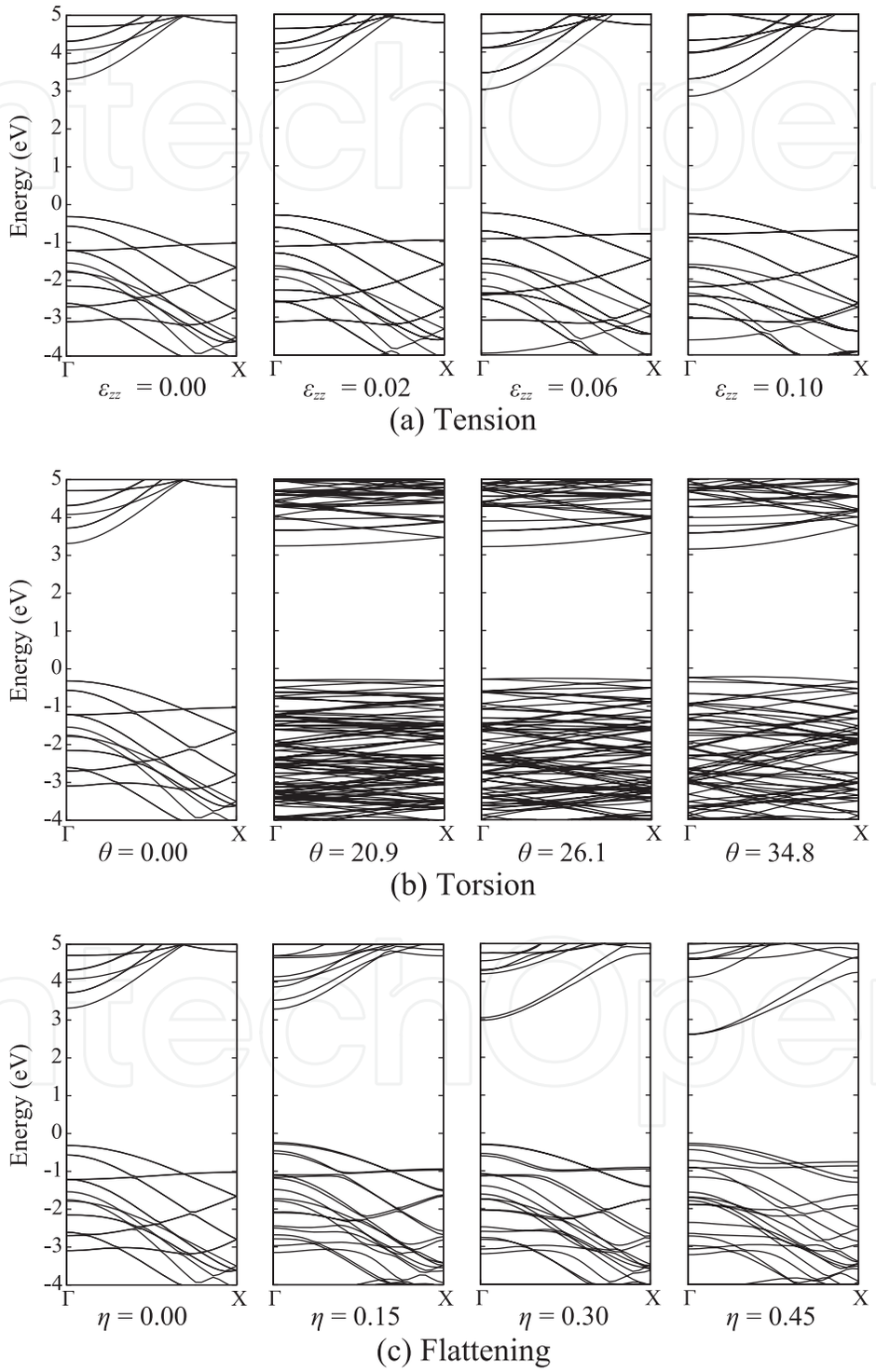

Figure 3. Change in the band structure of an (8,0) SWBNNT. The origin of the energy scale is set at the Fermi level.

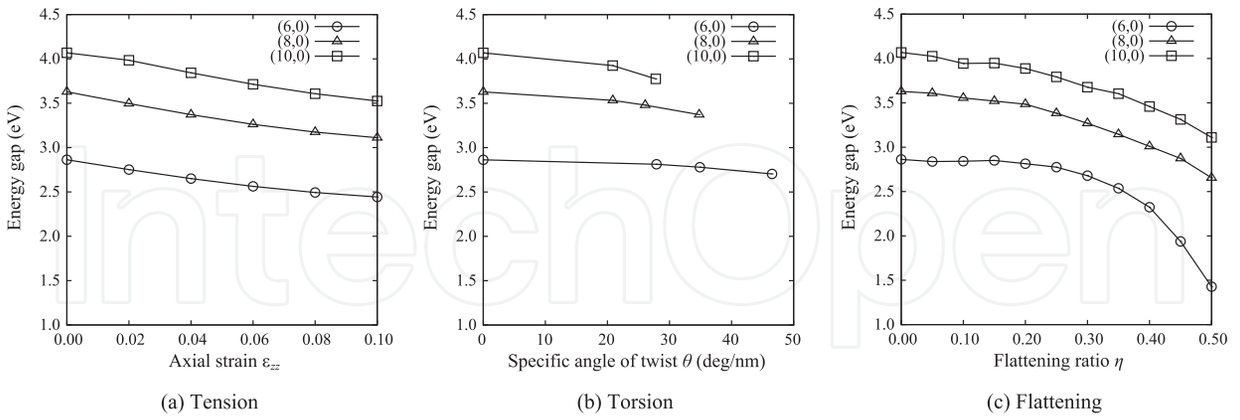

Figure 4. Energy gaps of the SWBNNTs as a function of (a) axial strain, (b) specific angle of twist, and (c) flattening ratio.

Figure 4 shows the energy gaps of the (6,0), (8,0), and (10,0) SWBNNTs as a function of the axial strain, specific angle of twist, and flattening ratio. The energy gap of the (10,0) with θ=41.7 deg/nm (N_z=5) is not shown in the figure because it collapsed. Under tension and torsion except for θ=20.8-27.8 deg/nm in the (10,0), the energy gap decreases almost linearly and the rate of decrease hardly depends on the diameter. In contrast, under flattening, the energy gap decreases quadratically or exponentially and the amount of decrease significantly depends on the diameter; a SWBNNT with the smaller diameter shows a larger decrease in the energy gap. It is also shown that flattening results in a few times larger decrease in the energy gap than tension and torsion.

Although the discussion so far in this section has dealt with the SWBNNTs under the three simple deformation modes, BNNTs would be subjected to combined deformation in their practical use. Therefore, the energy gap of the SWBNNTs subjected to flattening following axial tension is further analyzed (Figure 5). It is found that preceding tension shifts an E_g-η curve downward without dramatic changes in its shape, and that the extent of the shift almost corresponds to the energy gap decrease induced by simple tension (Figure 4(a)). This result suggests that the energy gap of the SWBNNTs under a combination of the three deformation modes can be deduced from Figure 4. In the rest of this section, therefore, only the simple deformation modes will be discussed.

2.2.2. Charge densities at the CBM

Here the mechanism of deformation-induced electronic changes in the SWBNNTs is discussed in terms of charge densities at the CBM (Figure 6). The CBM is composed of boron-derived states. In fact, CBM charge densities are high around boron atoms, while they are low around nitrogen atoms. It is found that the π^* state (p_z orbitals of boron atoms) hybridizes with the σ^*

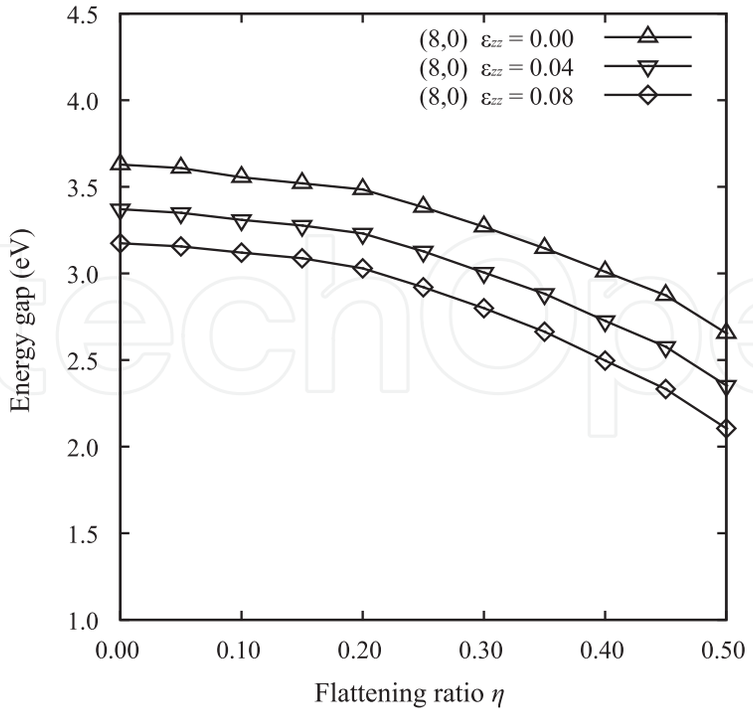

Figure 5. Change in the energy gap of (8,0) SWBNNT under flattening following axial tension.}

state along a circumference passing through boron atoms under no deformation (Figure 6(a), ε_{zz}=0.00), and that the tension, torsion, and flattening induce the change in the CBM state.

With increasing flattening deformation (Figure 6(d)), charges are transferred from the flattened to the curved regions, resulting in an overlap of the charge densities and formations of electronic bonds between neighboring boron atoms in the curved regions. It is this mechanism that results in the decrease in E_{CBM} in the flattened SWBNNTs. Comparing the three SWBNNTs with η=0.45 (Figures 6(d)-(f)), the electronic bonds become stronger as the diameter becomes smaller. Therefore, a flattened SWBNNT with a smaller diameter shows a larger decrease in the energy gap.

Under tension (Figure 6(a)), the tube curvature increases because of Poisson contraction, leading to the enhancement of π^*-σ^* hybridizations and the decrease in E_{CBM}. Figure 6(a) shows the narrowing white center area of zero-charge densities and the spreading gray area of π^*-σ^* hybridizations. The same is true for the torsion (Figure 6(b)), but it induces less change in charge densities than tension (the size of the white center area changes little in Figure 6(b)), resulting in a smaller decrease in the energy gap under torsion than under tension (Figures 4(a),(b)). It should be noted that elastic buckling occurred at a θ between 20.8 and 27.8 deg/nm in the (10,0), leading to local flattening (Figure 6(c)). Therefore, the relation of E_g versus θ deviates from the linear decrease at θ of 20.8-27.8 deg/nm in the (10,0) (Figure 4(b)). It is obvious that the overlap of charge densities is much stronger under flattening than under tension or torsion. Therefore, the decrease in the energy gap in the former is much larger than in the latter.

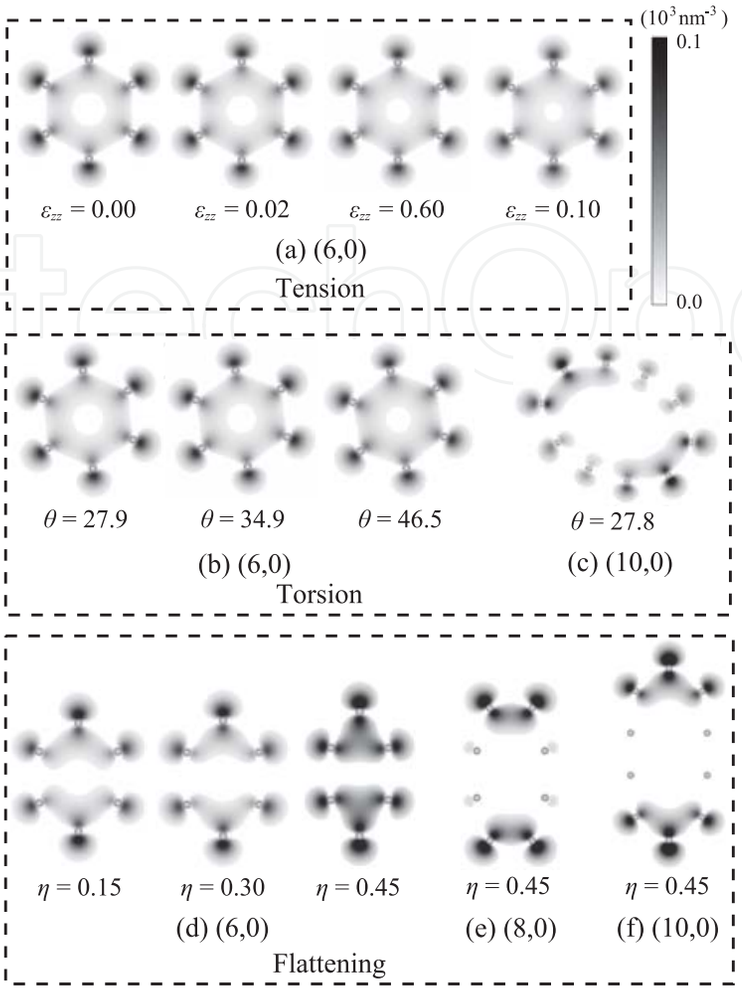

Figure 6. Change in the CBM charge density. Cross sections passing through boron atoms are shown.

2.2.3. Deformation forces

Figure 7 shows the deformation energy as a function of axial strain, specific angle of twist, and flattening ratio. The curves in tension, torsion, and flattening are fitted by cubic, quadratic, and quartic polynomials, respectively. The first and second derivatives of each curve provide the deformation force (Figure 8) and the elastic modulus, respectively. Young's moduli of the (6,0), (8,0), and (10,0) are thus calculated to be 0.759, 0.794, and 0.811 TPa, respectively. They are in good agreement with those measured in experiments (1.22±0.24 TPa [10] and 0.722 TPa [16]) and other first-principles calculations (0.762, 0.785, and 0.803 TPa for (6,0), (8,0), and (10,0), respectively [18]). It is found in Figure 8 that forces under flattening are smaller than under tension and torsion, because strong in-plane B-N covalent bonds prevent in-plane tension and torsion. It is also found that forces rapidly increase later under flattening. The rapid increase starts from around η=0.3 and 0.4 in the (6,0) and (8,0), respectively, where the imaginary wall distances are 0.35 and 0.38 nm, respectively. Because the interlayer distance of hexagonal BNs and MWBNNTs is around 0.34 nm, the rapid increase would be attributed to the repulsive force between the two flattened regions.

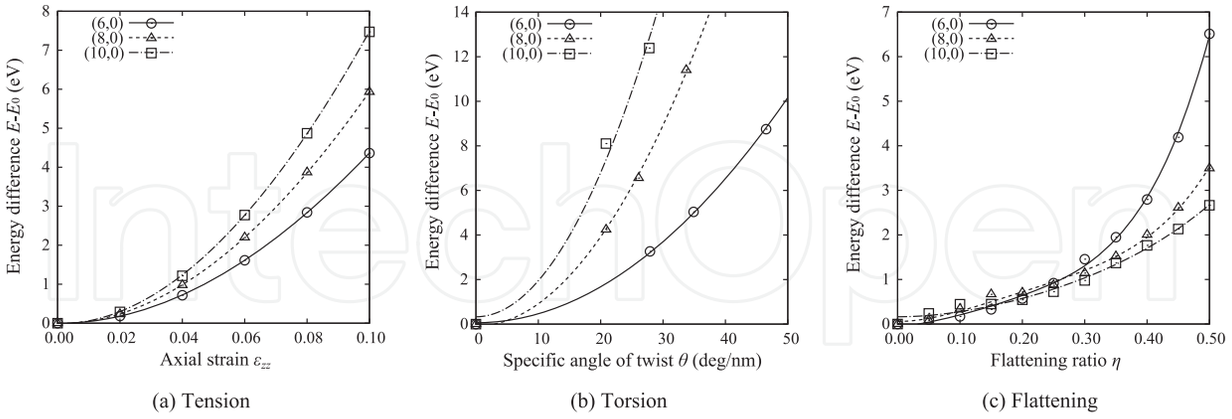

Figure 7. Deformation energy of the SWBNNTs as a function of (a) axial strain, (b) specific angle of twist, (c) flattening ratio.

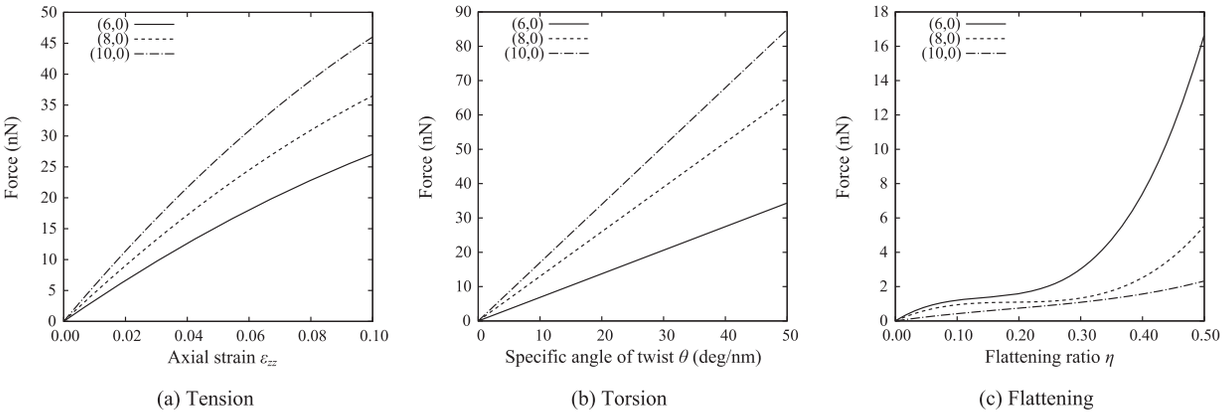

Figure 8. Forces required to deform (6,0), (8,0) and (10,0) SWBNNTs.

Figure 9 shows the relationship between energy gap and deformation force. The three bands to the right illustrate the obtainable range of the energy gap by introducing tension, torsion, and flattening. In tension and torsion, a larger force is required for a larger tube to induce the same amount of energy gap decrease. The opposite is true in flattening, i.e., a larger force for a smaller tube. The key findings from Figure 9 are that (i) the flattening with a force smaller than that applied for tension or torsion leads to the larger decrease in the energy gap, and (ii) flattening offers a larger obtainable range of the energy gap than tension and torsion: 1.4-4.0 eV under flattening, 2.5-2.8 eV and 3.1-4.0 eV under tension, 2.7-2.8 eV, 3.4-3.6 eV, and 3.8-4.0 eV under torsion. These findings indicate that flattening has the potential to enable BNNTs to be used as nanoelectronic devices. However, a valid question is whether flattening BNNTs is experimentally feasible.

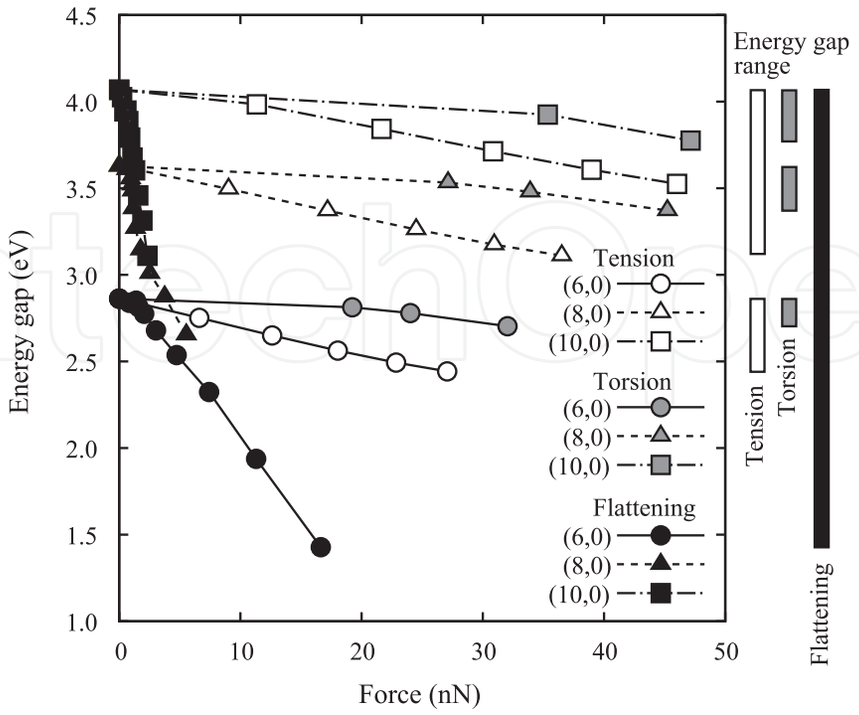

Figure 9. Relationship between energy gap and force of (6,0), (8,0) and (10,0) SWBNNTs.

In order to answer this question, the estimated flattening forces are compared with those of SWCNTs that Barboza et al. have already experimentally succeeded in flattening by means of an atomic force microscopy (AFM) tip [41]. Although they did not actually measure flattening forces of (*n*,0) SWCNTs with $n \leq 10$, they proposed and validated a universal relationship among the applied force, SWCNT diameter, AFM tip radius, and flattening ratio:

$$\frac{F D_0^{3/2}}{(2R)^{1/2}} = \frac{\alpha}{(1-\eta)^{3/2}}\left[\sqrt{2\eta+\eta^2} + tg^{-1}\left(\sqrt{\frac{\eta}{1-\eta}}\right)\right] \tag{5}$$

where R is the AFM tip radius and α is a constant (=1.2×10^{-18} J). Equation (5) indicates that the quantity $FD_0^{3/2}(2R)^{-1/2}$ should be universal to any SWCNT. They showed that all experimental data fall on a single curve obtained by Equation (5) up to $\eta \cong 0.4$. From Equation (5) and the geometric contact conditions between a tube and an AFM tip, the flattening force per unit length of a (6,0) SWCNT (D_0=0.470 nm) is calculated to be 15.4 N/m when η=0.4 and R=30 nm. In contrast, from Figure 8, that of the (6,0) SWBNNT (=F/L_{z0}) is estimated to be 16.8 N/m at η=0.4. The results demonstrate that the flattening force is almost equal in SWCNTs and SWBNNTs, indicating that the same experiments as Barboza et al. would be feasible for SWBNNTs. The fact that CNTs and BNNTs almost have the same tube shape and size when their chiral indexes are the same ($a \cong 0.142$ nm in CNTs and $a \cong 0.145$ nm in BNNTs) also encourages the feasibility of flattening BNNTs. It is therefore concluded that the flattening forces estimated are not unrealistic and strongly expected that the same or similar experimental technique also applies to BNNTs.

3. MWBNNTs under flattening

3.1. Simulation procedure

This section focuses on (5,0), (13,0), and (21,0) SW, (5,0)@(13,0) and (13,0)@(21,0) DW, and (5,0)@(13,0)@(21,0) TWBNNTs. Figure 10 shows the simulation model of the (13,0)@(21,0) DWBNNT. The initial nearest interatomic distance between boron and nitrogen atoms is set as 0.145 nm. Boron (nitrogen) atoms in the outer tube are stacked above nitrogen (boron) atoms in the inner tube [42]. The axial direction of the BNNT is parallel to the *z*-direction. The BNNT is located at the center of the unit cell with a size of 3.637 nm × 3.637 nm × 0.435 nm. Even though a three-dimensional periodic boundary condition is employed, the cell sizes in the *x*- and *y*-directions are large enough to avoid interaction with neighboring image cells, because they have little effect (less than 1%) on the energy, charge distribution, and energy band structure of a flattened BNNT, when they are greater than the diameter of the BNNT plus 1.0 nm.

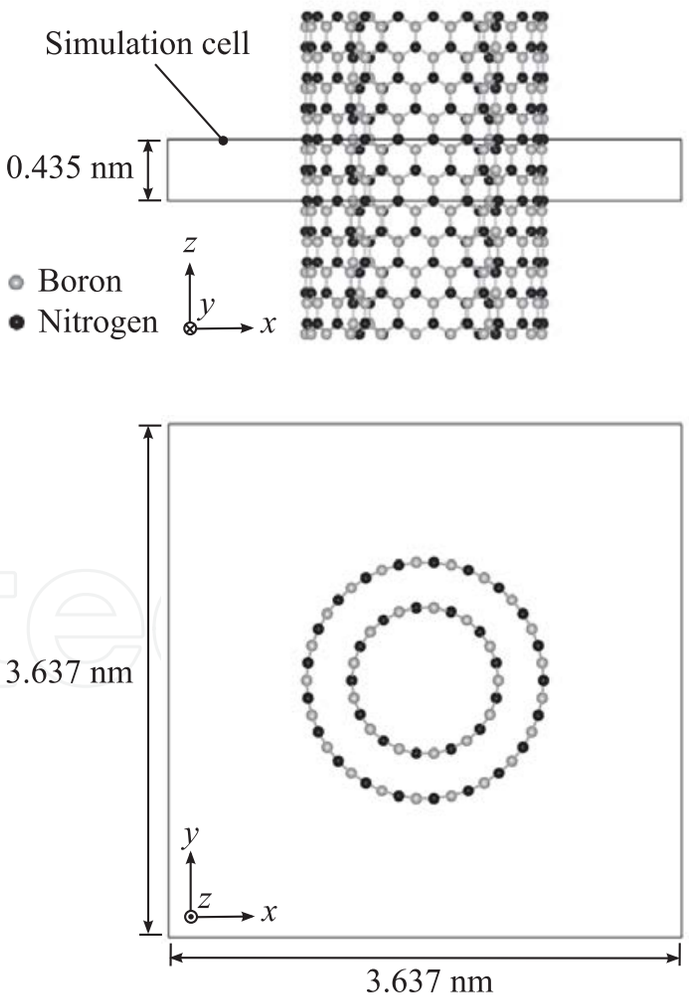

Figure 10. Simulation model of (13,0)@(21,0) DWBNNT.

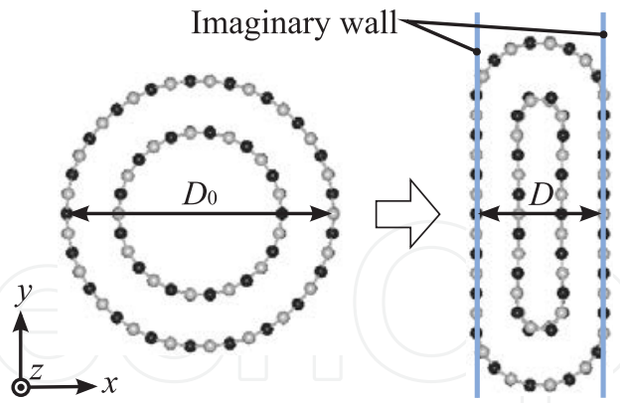

Figure 11. Schematic illustration explaining flattening compression of BNNTs.

Atomic positions and the cell size in the *z*-direction are first relaxed using the conjugate gradient method until atomic forces and the stress component, σ_{zz}, become less than 0.01 eV/Å and 0.01 GPa, respectively. After obtaining the equilibrium structure, a flattening compression in the *x*-direction is applied by reducing the distance between imaginary walls until the BNNT collapses (Figure 11). Once an atom contacts a wall, the atom is allowed to move only on the wall. During compression, the cell sizes are fixed and atomic configurations are relaxed until their forces become less than 0.01 eV/Å. To investigate the degree of deformation, the flattening ratio, η, is defined as

$$\eta = \frac{D_0 - D}{D_0} \tag{6}$$

where D_0 is the diameter of the outermost tube at equilibrium, and D is the distance between the imaginary walls.

First-principles DFT calculations are conducted using the Vienna Ab Initio Simulation Package (VASP) [32, 33]. The wave functions are expanded in a plane-wave basis set with a cut-off energy of 350 eV. The ultrasoft pseudopotential proposed by Vanderbilt [34] is used, and the exchange-correlation energy is evaluated by the generalized gradient approximation of Perdew and Wang [35]. The Brillouin zone integration is performed by the Monkhorst-Pack scheme [36] using a 1 × 1× 4 *k*-point mesh.

3.2. Results and discussion

3.2.1. Energy-band structures

Figure 12 shows the change in the energy band structures of the (13,0) SWBNNT and (13,0)@(21,0) and (5,0)@(13,0) DWBNNTs during flattening deformation. The other SWBNNTs and the (5,0)@(13,0)@(21,0) TWBNNT show a similar changing trend of the band structure to the (13,0) SWBNNT and the (5,0)@(13,0) DWBNNT, respectively. Both the valence band maximum (VBM) and the conduction band minimum (CBM) of the (13,0) SWBNNT and

(13,0)@(21,0) DWBNNT are located at the Γ point (k=0) during the deformation, but those of the (5,0)@(13,0) DWBNNT move to $k\neq0$ midway during the deformation and then return to the Γ point. In each BNNT, the energy of the VBM, E_{VBM}, hardly changes, while that of the CBM, E_{CBM}, changes, indicating that the change in the energy gap, E_g, is mainly caused by a change in E_{CBM}. In the (13,0) SW and (13,0)@(21,0) DWBNNTs (Figure 12(a), (b)), E_{CBM} decreases monotonically. In contrast, in the (5,0)@(13,0) DWBNNT (Figure 12(c)), E_{CBM} first increases and then decreases.

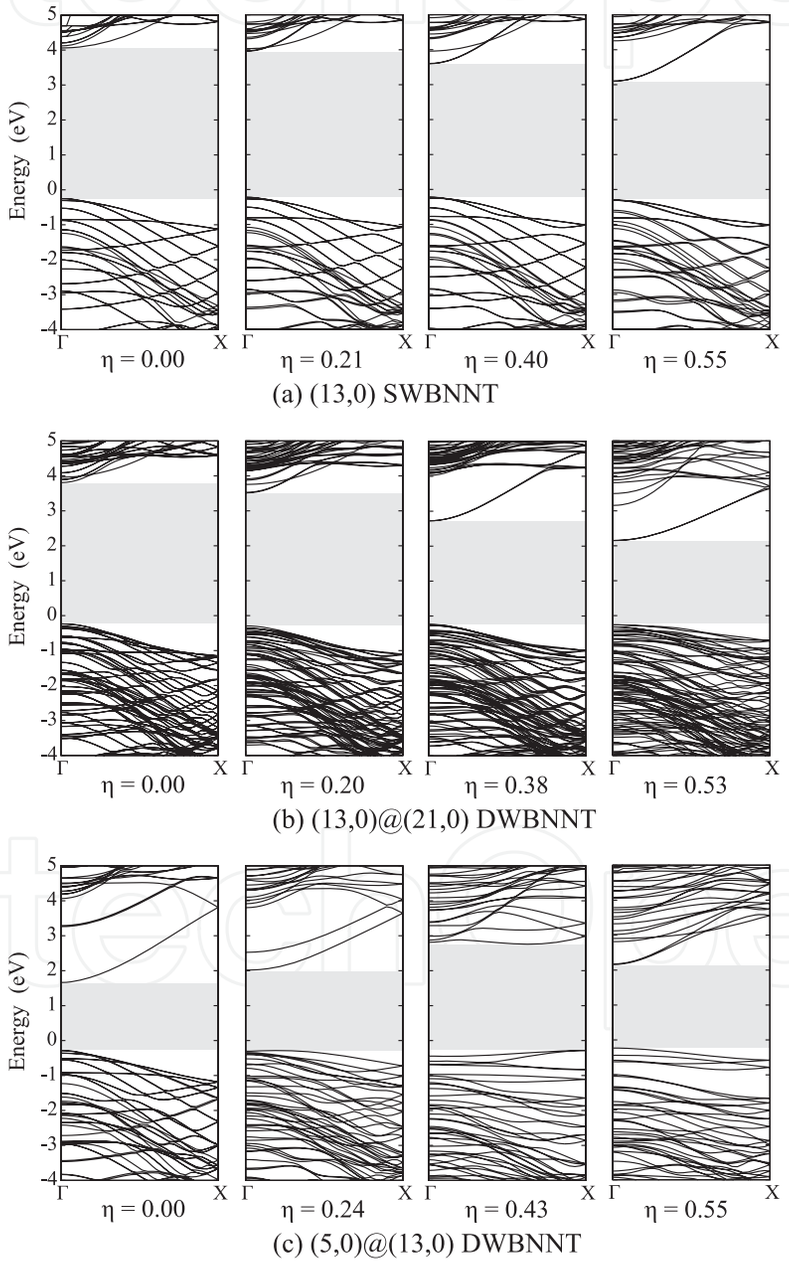

Figure 12. Change in the band structure of (13,0) SWBNNT and (13,0)@(21,0) and (5,0)@(13,0) DWBNNTs in flattening deformation. The origin of the energy scale is set at the Fermi level.

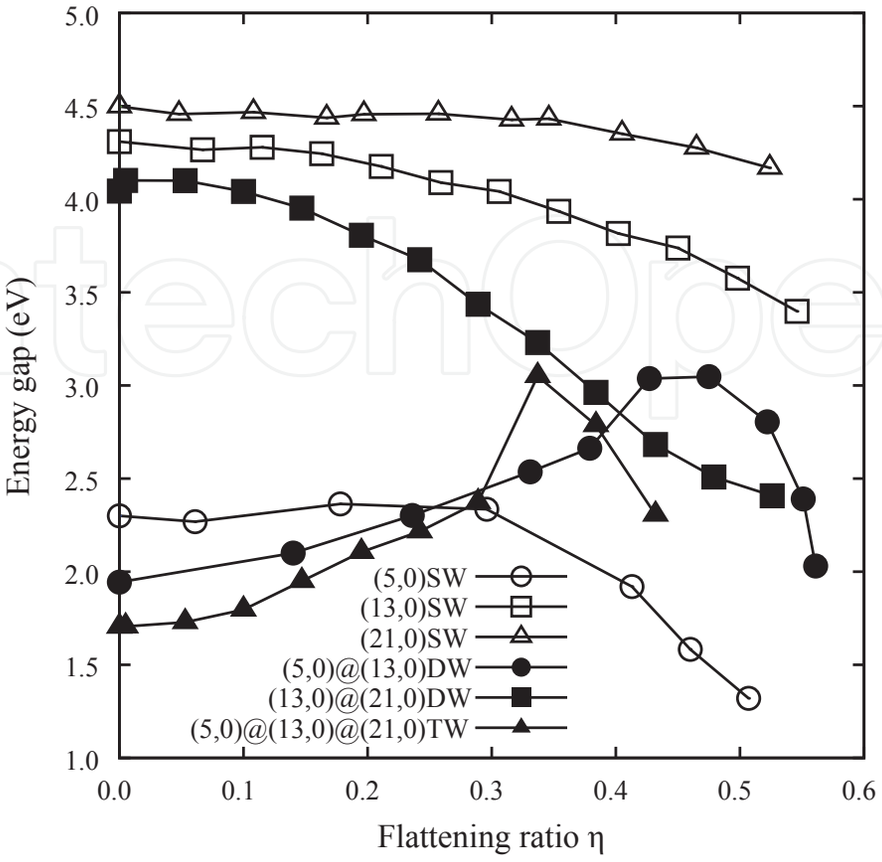

Figure 13. Relationship between energy gap, E_g, and flattening ratio, η, of (5,0), (13,0), and (21,0) SWBNNTs, (5,0)@(13,0) and (13,0)@(21,0) DWBNNTs, and (5,0)@(13,0)@(21,0) TWBNNT.

Figure 13 shows the energy gaps of the (5,0), (13,0), and (21,0) SWBNNTs, (5,0)@(13,0) and (13,0)@(21,0) DWBNNTs, and (5,0)@(13,0)@(21,0) TWBNNT as a function of the flattening ratio. The energy gap of the three SWBNNTs decreases almost monotonically, and the amount of decrease becomes smaller with increasing tube diameter. The energy gap of the (13,0)@(21,0) DWBNNT also decreases monotonically, but it exhibits a more rapid decrease than the (13,0) and (21,0) SWBNNTs. It should be noted that the energy gaps of the (5,0)@(13,0) DWBNNT and (5,0)@(13,0)@(21,0) TWBNNT increase during the early stage and then decrease. This shift occurs earlier in the latter (η=0.34) than in the former (η=0.48). The fact that the (5,0)@(13,0) DWBNNT and (5,0)@(13,0)@(21,0) TWBNNT show different changing trends of E_g from the SWBNNTs proves that interwall interactions significantly affect the electronic structures of the flattened (5,0)@(13,0) DWBNNT and (5,0)@(13,0)@(21,0) TWBNNT.

3.2.2. Charge densities at the CBM

Figure 14 shows charge densities at the CBM of the flattened (5,0), (13,0), and (21,0) SWBNNTs at a cross section passing through boron atoms. The characteristics of the nearly free electron (NFE) state are observed in the BNNTs with a small curvature (Figure 14(b): η=0.00, (c): η=0.00, 0.20), while π^*-σ^* hybridizations appear in the others. The reason the CBM of the (13,0) and

(21,0) SWBNNTs changes from a NFE-like state to a π^*-σ^* hybridized state is that the tube curvature increases locally as the flattening deformation increases (in (n,0) SWBNNTs under no deformation, the CBM is a NFE-like state when $n \geq 13$ and a π^*-σ^* hybridized state when $n < 13$, and the hybridization becomes stronger with increasing tube curvature) [8]. The energy gap of the (5,0) SWBNNT is much smaller than those of the (13,0) and (21,0) SWBNNTs because of its strong π^*-σ^* hybridization. With increasing flattening deformation, charge is transferred from flattened regions to curved ones, leading to an overlap of the charge densities. The E_{CBM} of the SWBNNTs decreases under flattening because of the formation of electronic bonds between neighboring boron atoms in the curved regions. The charge density distribution in curved regions of the (13,0) SWBNNT at η=0.21 is similar to that of the (21,0) SWBNNT at η=0.52, which results in them having almost the same energy gap of 4.2 eV. This is because they have almost the same value of D, namely the same curvature of the curved region. Figure 15 shows the relationship between the energy gap and imaginary wall distance of the (13,0) and (21,0) SWBNNTs. Their energy gaps are almost equal under a same wall distance.

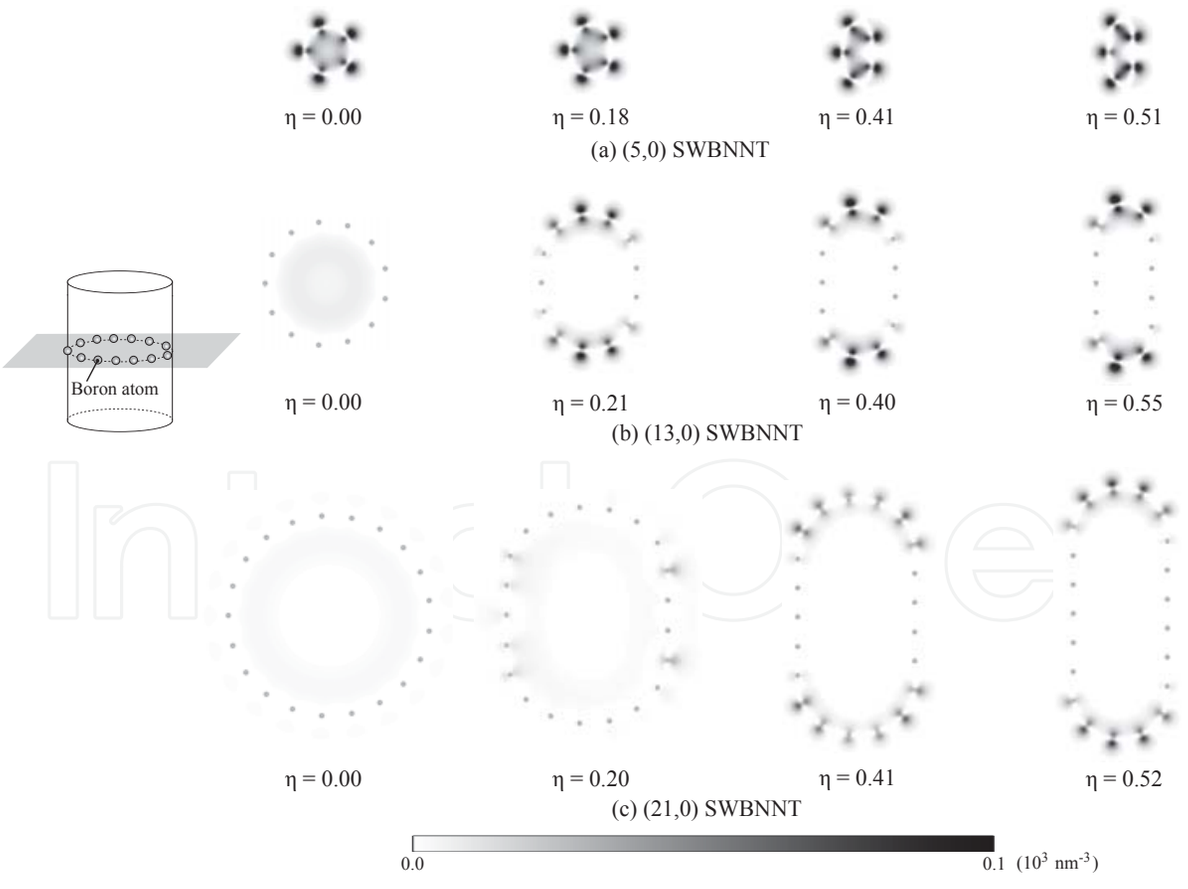

Figure 14. Change in the CBM charge density of (5,0), (13,0), and (21,0) SWBNNTs in flattening deformation.

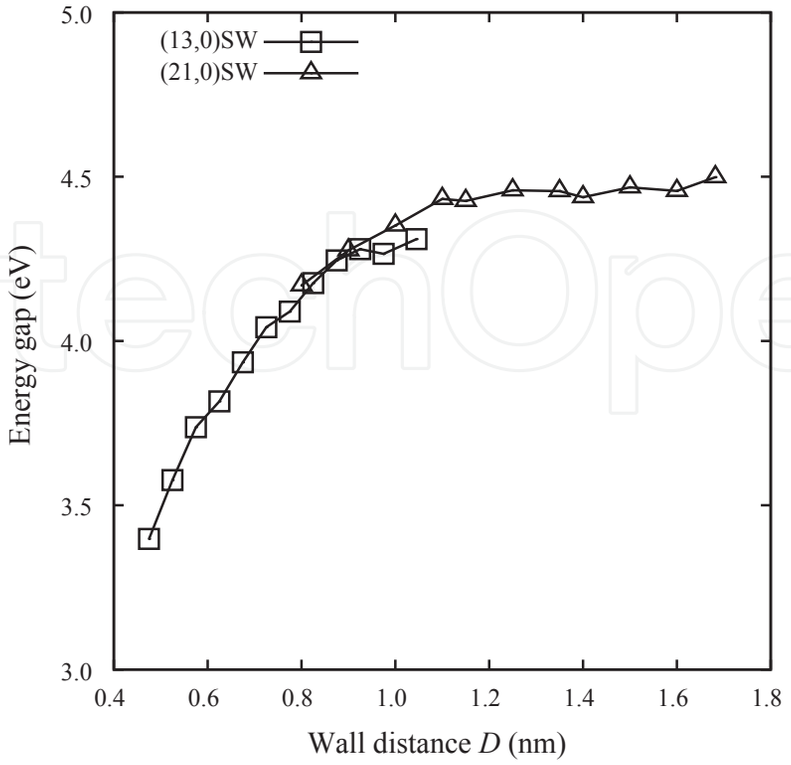

Figure 15. Energy gap of (13,0) and (21,0) SWBNNTs as a function of imaginary wall distance.

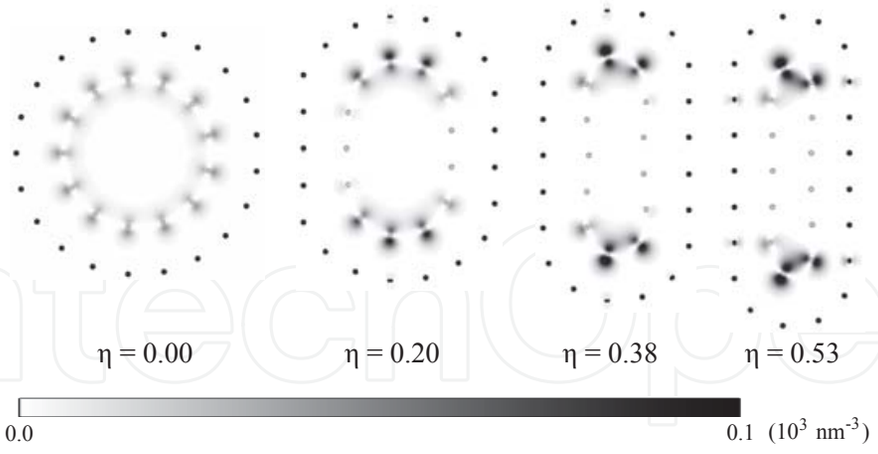

Figure 16. Change in the CBM charge density of (13,0)@(21,0) DWBNNT during flattening deformation.

The CBM charge density distribution of the (13,0)@(21,0) DWBNNT is similar to that of the SWBNNTs (Figure 16). In the inner tube, charge transfer from flattened to curved regions is observed and an overlap of the charge densities is induced in the curved regions. The decrease in E_{CBM} of the (13,0)@(21,0) DWBNNT is caused by the same mechanism as in the SWBNNTs mentioned above. Because the charge densities are distributed almost entirely in the inner tube

during deformation, one might expect that the E_g-η curve of the (13,0)@(21,0) DWBNNT coincides with that of the (13,0) SWBNNT. However, E_g of the former is in fact smaller than that of the latter under the same η. As shown in Figure 16, the flattening ratio of the innermost tube, η_{in}, must be larger than η to maintain the interwall spacing constant. This means that the B-B bonds in the flattened (13,0)@(21,0) DWBNNT are stronger than those in the flattened (13,0) SWBNNT under the same η, resulting in a larger decrease in E_{CBM} in the former than in the latter.

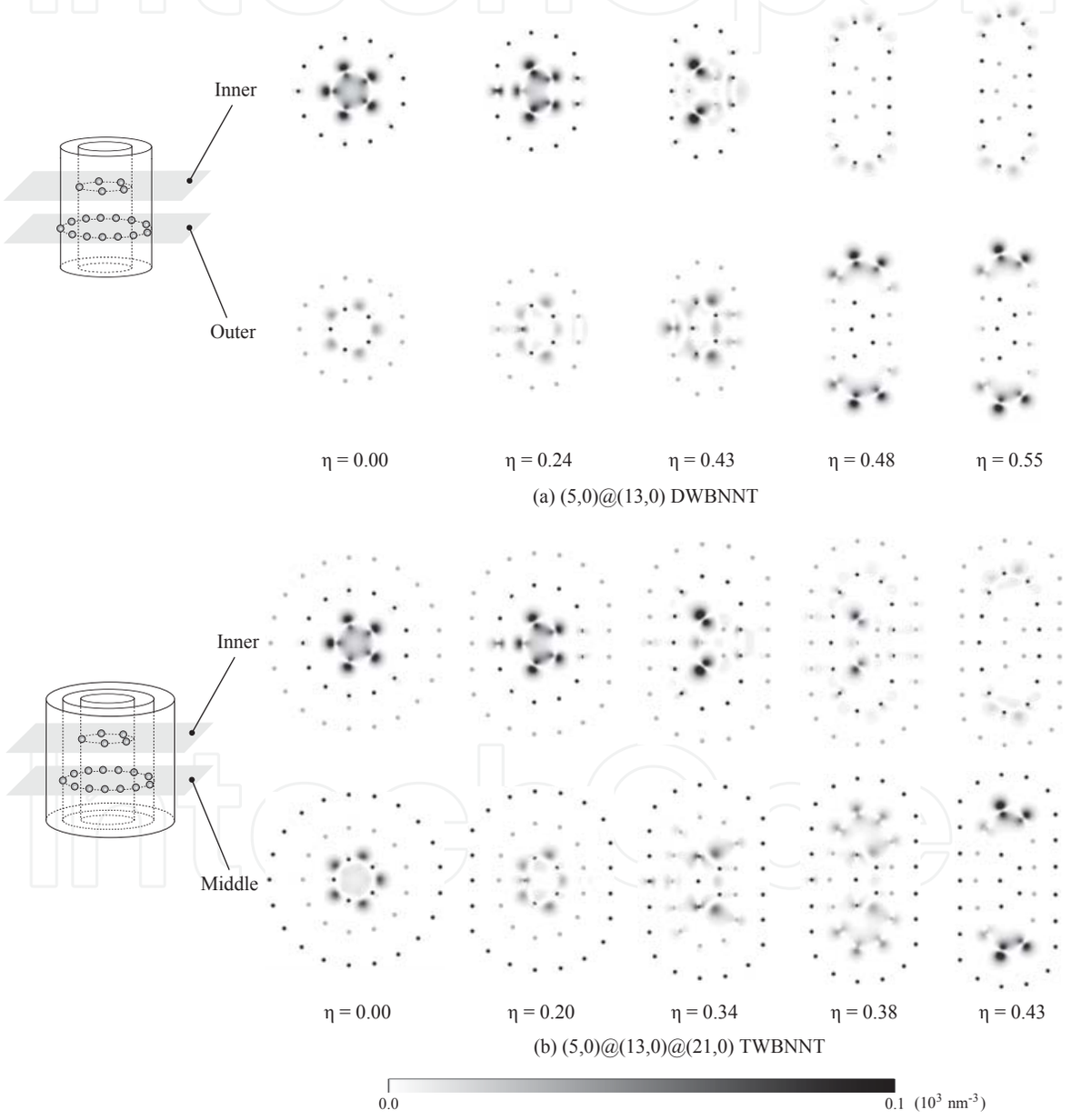

Figure 17. Change in the CBM charge density of (5,0)@(13,0) DWBNNT and (5,0)@(13,0)@(21,0) TWBNNT during flattening deformation.

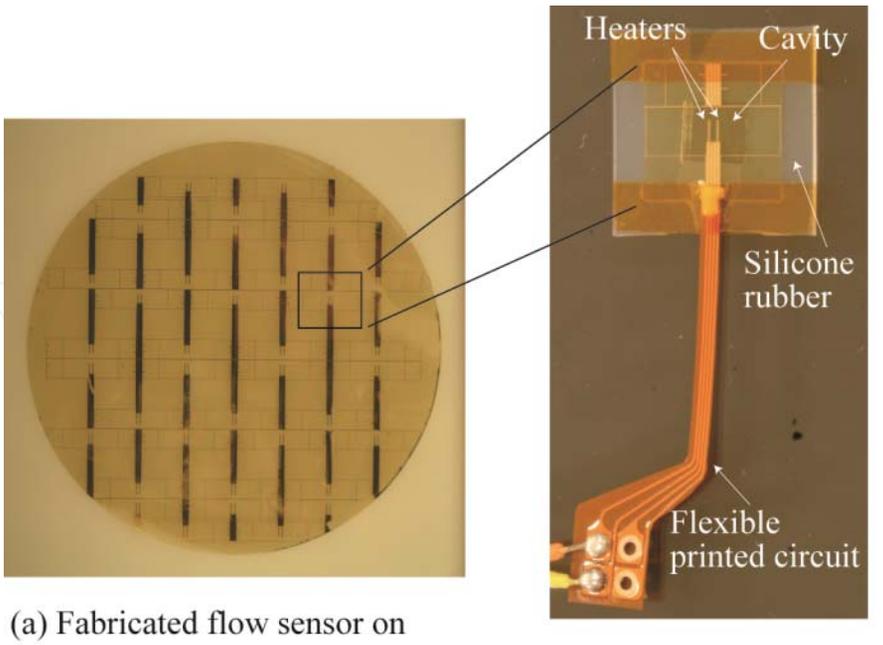

Figure 7. Patch-type flexible flow sensor for large scale air-conditioning network systems.

which enables us to calculate the flow rate values from the obtained sensor outputs in bent ducts, was derived [38].

3.3. Flow sensors for medical applications

The numbers of cardiac disease and cerebral stroke patients are gradually decreasing, thanks to developments in medical devices and improved health guidance. However, chronic obstructive pulmonary disease (COPD) is still on the increase. Spirometry is normally used to evaluate the progress of COPD. It measures the flow rate in the human mouth. The respiratory system consists of numerous levels of bronchi just like a tree, and the lung alveoli are located at the end of diverging bronchi. In the case of COPD, the alveoli structures gradually collapse as the patient ages and because of absorbed cigarette smoke or other air-polluting substances. Lesions develop at the ends of the diverging bronchi. The current method of measurement, which evaluates lesions in the mouth, cannot be used to evaluate such small lesions in the bronchi.

To overcome the above problem, Shikida et al. [34, 39] devised a catheter-type flow sensor that can measure aspirated- and inspired-air flow characteristics trans-bronchially. The flow sensor (Figure 8) can be inserted into a small bronchus for measuring aspirated and inspired air characteristics. An on-wall in-tube thermal flow sensor is mounted on the inside of the tube, and it is used in the bronchoscope. The external diameter of the tube is only a few mm, and therefore, it can reach into the small bronchus. Two heaters were formed on the film in order to detect the flow direction.

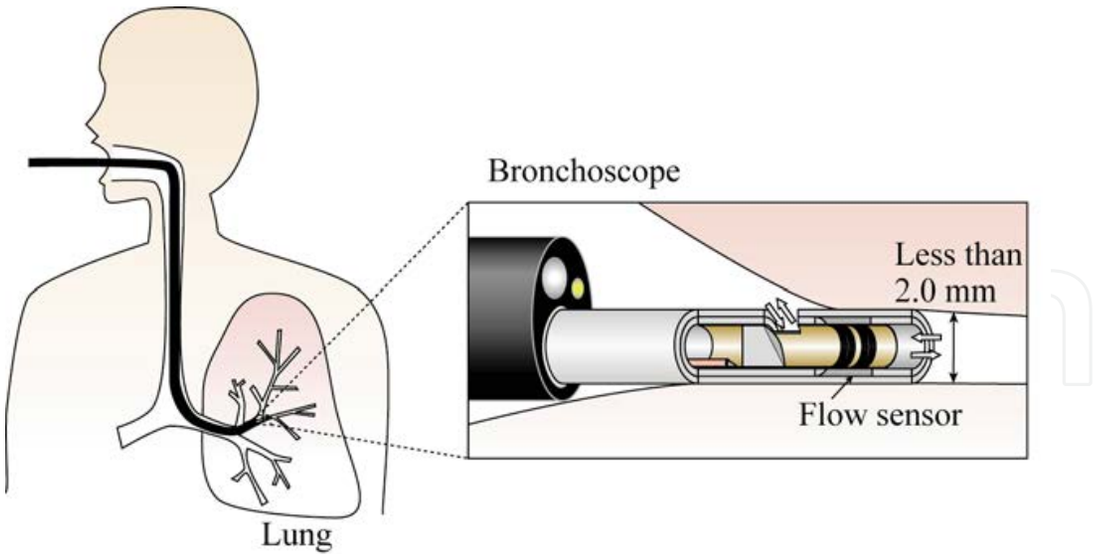

Figure 8. Concept of catheter flow sensor for trans-bronchial measurement. Republished with permission of IOP Published Ltd from Ref. [34].

Polymer-MEMS technologies and heat shrinkable tubes are used to produce the sensor. The fabrication process consists of two steps.

1. Flexible film sensor fabrication

Polyimide film is used as a substrate. The thickness of the film affects the thermal response performance (it has to be relatively thick; 7.5 μm). The metal film heater structures are formed on the film by using photolithography and sputtering, and they are patterned with a lift-off process. The typical size of the sensor is 2.8 mm x 5.5 mm. Two heaters are formed on the film in order to detect the flow direction. Each film sensor is mechanically cut before being mounted inside the tube.

2. Mounting film sensor inside a tube

The sensor is mounted on the inside surface of the tube as follows.

a. The sensor is inserted into a heat shrinkable tube made of Teflon.

b. The heat shrinkable tube is baked at 110°C. The Teflon tube shrinking to almost half its original size as a result of heating, and the film sensor is automatically mounted on the inner wall surface during the shrinking process and becomes fixed on the tube surface.

c. A cavity structure is formed under the heating element to improve thermal isolation. To produce the active structure, a slit is formed on the tube, and it is covered with a one-mode Teflon heat-shrinkable tube to seal it. The outer diameter of the inner tube is only a little bit larger than the inner diameter of the outer one, after the heat shrinking process. Thus, these two Teflon tubes are tightly fixed to one other.

Figures 9(a) and 9(b) show a schematic diagram and a photograph of the fabricated catheter-type flow sensor. The inner and outer diameters of the tube are 1.0mm and 1.8 mm. The

temperature coefficient of resistance of the sensor is $0.0025K^{-1}$. The package method of the on-wall in-tube film mounting is suitable for miniaturization because the sensor structure itself does not disturb the flow stream.

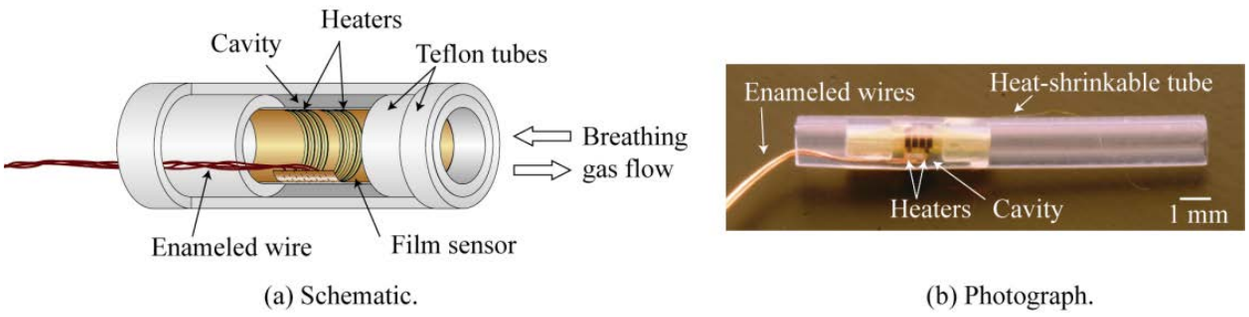

Figure 9. Fabricated catheter type flow sensor. Republished with permission of IOP Published Ltd from Ref. [39].

Experiments were done under the regulations set out in the Nagoya University Animal Experiments Guidelines, and they were approved by the animal ethics committee. The experiments were done under anesthesia. Thus, the following data are aspirated- and inspired-air characteristics under anesthesia. Infiltration of bodily fluids into the tube was prevented by using Teflon as the tube material. The catheter flow sensor is intended to be incorporated into a bronchoscope and to be inserted in the small airways from the mouth. Thus, the sensor was first tested on rats. An optical fiberscope with an outer diameter of 0.8 mm, instead of a bronchoscope, was used in the tests. Inserting the flow sensor into the airway from the mouth of the rat with the fiberscope involved three steps.

1. Only the fiberscope was inserted, from the mouth to the targeted location, by observing the inside of the airway. Then, the sensor was inserted to the targeted location with a Teflon tube guide.
2. The fiberscope was withdrawn when the flow sensor reached the target location.
3. The Teflon tube guide was carefully extracted and only the flow sensor remained at the location.

The breathing waveform of the rat is shown in Figure 10. A period of 820 ms for inspiration and aspiration was obtained. This means that the respiration frequency was 1.1 Hz. The ventilated air volume was calculated from this breathing waveform, and a value ranging from 1.01–1.09 cc was obtained. The known respiration frequency and ventilated air values of rats range from 1.1–1.9 for the former and from 0.60–1.25 for the latter. The measured values coincided with the physiological values in the literature.

The air was inspired for a short time period, suddenly becoming aspirated for a time period. In aspirated mode, a large amount of air was aspirated at the beginning, and the aspirated air gradually decreased afterwards. Inspiration and aspiration were done by moving the diaphragm. The air was inspired by expanding the thoracis. This was done by contracting the diaphragm. The air was simply aspirated by the restorative force of the thoracis. Thus, the air

was inspired in a short time, and a large amount of air was aspirated at the beginning of the aspiration mode, and the amount gradually decreased after that. The sensor signal quantitatively corresponded to this natural respiratory mechanism. From these results, the catheter flow sensor will be useful for evaluating the flow characteristics in the small bronchus region in the future.

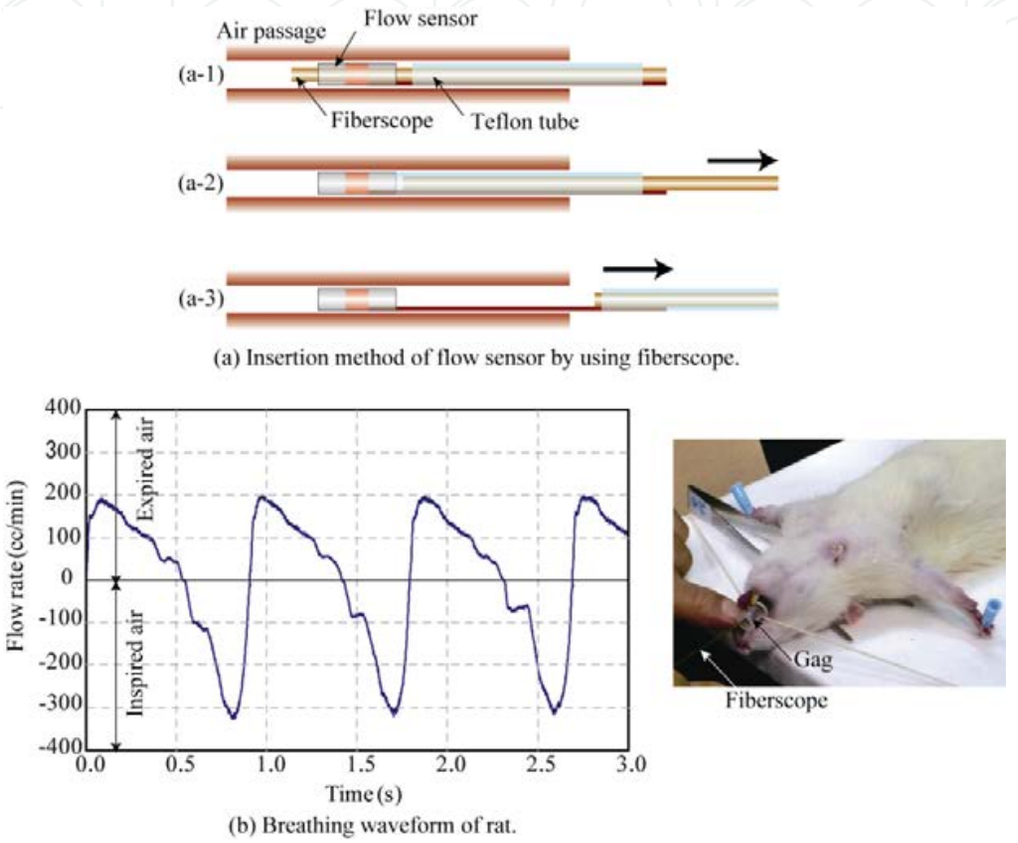

Figure 10. Breathing waveform of rat measured with intubated catheter flow sensor. Republished with permission of IOP Published Ltd from Ref. [39].

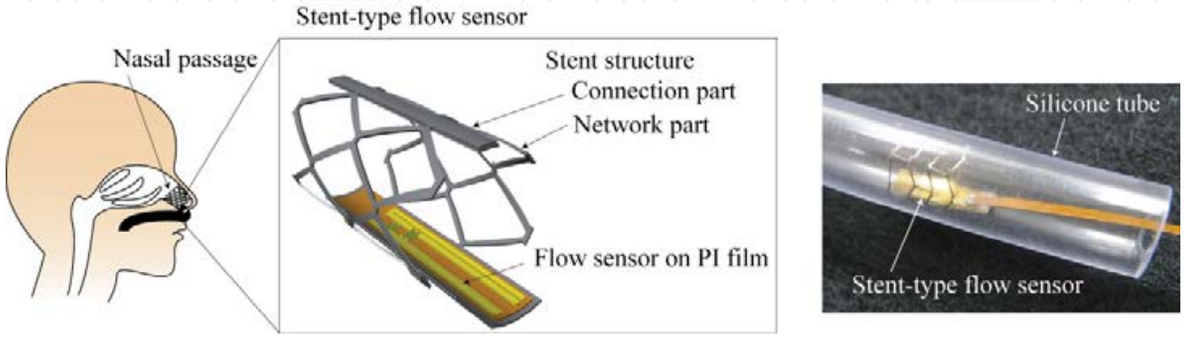

Figure 11. Stent flow sensor for evaluation of nasal respiration. Republished with permission of IOP Published Ltd from Ref. [40].

A human being breathes through the mouth and the nose. Bacteria and viruses are trapped in the nose cavity, and only clean inspired air is supplied to the hung. The inspired air is also humidified in the cavity in order for lungs to adsorb oxygen effectively. The inspired air is warmed inside the body is then expired outside; this is a method of heat exchange. The flow characteristics of the nose are deeply related to various health concerns. Thus, a stent-type of thermal flow sensor was also developed for measuring nasal respiration. The MEMS stent flow sensor is shown in Figure 11. It is a thermal flow sensor fabricated on polymer film and monolithically integrated on the stent structure [40].

4. Conclusion

This chapter described the fabrication and applications of micro-sensors produced by MEMS technologies. The attractive features and problems of MEMS sensors were discussed. In particular, MEMS sensors have low costs, high space and time resolutions, and reduced dead space. The applications of MEMS sensors include tactile Si-solid and fabric sensors for human interfaces and flow sensors for air-conditioning systems and medicine.

Acknowledgements

The research was supported by the Centre of Excellence (COE) for Education and Research on Micro-Nano Mechatronics and a Grant-in-Aid for Scientific Research (B) No. 23310091 from the Ministry of Education, Culture, Sports, Science and Technology (MEXT), Japan.

Author details

Mitsuhiro Shikida

Department of Micro-Nano Systems Engineering, Nagoya University, Nagoya, Japan

References

[1] Petersen K. E. Silicon as a mechanical material. Proceedings of the IEEE 1982;70(5) 420-457.

[2] Muller R. S, Howe R. T, Senturia S. D, Smith R. L, White R. M. Microsensor. USA: IEEE PRESS; 1990.

[3] Yamasaki H., editor. Handbook of sensors and actuators – Intelligent sensors (vol. 3). The Netherlands: Elsevier Science B. V.; 1996. 3.

[4] Ristic L. Sensor technology and devices. USA: Artech House, Inc.; 1994.

[5] Maluf N. An introduction to microelectromechanical systems engineering. USA: Artech House, Inc.; 2000.

[6] Chu Z, Sarro P. M, Middlehoek S. Silicon three-axial tactile sensor, In: Technical Digest of The 8th International Conference on Solid-State Sensors and Actuators, June 1995, Stockholm, Sweden; 1995.

[7] Kane B. J, Cutkosky M. R, Kovacs G. T. A. A traction stress sensor array for use in high-resolution robotic tactile imaging. Journal of microelectromechanical systems 2000;9(4) 425-434.

[8] Kasten K, Amelung J, Mokwa W. CMOS-compatible capacitive high temperature pressure sensors. Sensors and Actuators A: Physical 2000;85(1-3) 147-152.

[9] Kim K, Lee K. R, Kim Y. K, Lee D. S, Cho N. K, Kim W. H, Park K. B, Park H. D, Park Y. K, Kim J. H, Pak J. J. 3-axes flexible tactile sensor fabricated by Si micromachining and packaging technology. In: Proceedings of IEEE MEMS'06. January 2006, Istanbul, Turkey; 2006.

[10] Takao H, Yawata M, Sawada K, Ishida M. A robust and sensitive silicon-MEMS tactile-imager with scratch resistant surface and over-range protection. Technical Digest of The 14th International Conference on Solid-State Sensors, Actuators and Microsystems. June 2007, Lyon, France; 2007.

[11] Shikida M, Shimizu T, Sato K, Itoigawa K. Active tactile sensor for detecting contact force and hardness of an object. Sensors and Actuators A: Physical 2003;103(1-2) 213-218.

[12] Hasegawa Y, Shimizu T, Miyaji T, Shikida M, Sasaki H, Sato K, Itoigawa K. A micromachined active tactile sensor for hardness detection. Sensors and Actuators A : Physical 2004;114(2-3) 141-146.

[13] Hasegawa Y, Shikida M, Sasaki H, Sato K, Itoigawa K. An active tactile sensor for detecting mechanical characteristics of contacted objects. Journal of micromechanics and microengineering 2006;16(8) 1625-1632.

[14] Engel J, Chen J, Liu C. Development of polyimide flexible tactile sensor skin. Journal of micromechanics and microengineering 2003;13(3) 359-366.

[15] Kim S-H, Engel J, Liu C, Jones D. L. Texture classification using a polymer-based MEMS tactile sensor. Journal of micromechanics and microengineering 2005;15(5) 912-920.

[16] Lee H-K, Chang S-I, Yoon E. A flexible polymer tactile sensor: Fabrication and modular expandability for large area deployment. Journal of microelectromechanical systems 2006;15(6) 1681–1686.

[17] Hwang E-S, Seo J-H, Kim Y-J. A polymer-based flexible tactile sensor for both normal and shear load detections and its application for robotics. Journal of microelectromechanical systems 2007;16(3) 556–563.

[18] Konishi S, Maeda H, Ezaki T, Kawato M, Asajima S, Makikawa M. A selective stimulation of nerve bundles using a flexible multielectrode. In: Technical Digest of The 10th International Conference on Solid-State Sensors and Actuators. June 1999, Sendai, Japan; 1999.

[19] Chen N, Engel J, Pandya S, Liu C. Flexible skin with two-axis bending capability made using weaving by-lithography fabrication method. In: Proceedings of IEEE MEMS'06, January, 2006, Istanbul, Turkey; 2006.

[20] Hasegawa Y, Shikida M, Ogura D, Sato K. Glove type of wearable tactile sensor produced by artificial hollow fiber. In: Technical Digest of The 14th International Conference on Solid-State Sensors, Actuators and Microsystems. June 2007, Lyon, France; 2007.

[21] Hasegawa Y, Shikida M, Ogura D, Suzuki Y, Sato K. Fabrication of a wearable fabric tactile sensor produced by artificial hollow fiber. Journal of micromechanics and microengineering 2008;18(8) 085014 .

[22] Kita G, Suzuki Y, Shikida M, Sato K. Fabric tactile sensor composed of ball-shaped umbonal fiber for detecting normal and lateral force. Micro & Nano Letters 2010;5(4) 211-214.

[23] Kita G, Shikida M, Suzuki Y, Tsuji Y, Sato K. Large-sized fabric tactile sensors for detecting contacted objects. Micro & Nano Letters 2010;5(6) 389-392.

[24] Liu C, Huang J-B, Zhu Z, Jiand F, Tung S, Tai Y-C, Ho C-M. A micromachined flow shear-stress sensor based on thermal transfer principle. Journal of Microelectromechanical systems 1999;8(1) pp. 90-99.

[25] Zhe J, Midi V, Farmer Jr K. R. A microfabricated wall shear-stress sensor with capacitative sensing. Journal of Microelectromechanical systems 2005;14(1) 167-175.

[26] Unnikrishnan S, Jansen H. V, Berenschot J. W, Mogulkoc B, Elwenspoek M. C. MEMS within a Swagelok®: a new platform for microfluidic devices. Lab on a Chip 2009;9(13) 1966-1969.

[27] Gianchandani Y, Tabata O, Zappe H. Comprehensive MEMS, Elsevier Science B. V. 2008.

[28] Elwenspoek M, Wiegerink R. Mechanical microsensors. Germany, Springer; 2001.

[29] Zhu R, Liu P, Liu X. D, Zhang F. X, Zhou Z. Y. A low-cost flexible hot-film sensor system for flow sensing and its application to aircraft. Technical Digest IEEE Micro Electro Mechanical Systems Conference. January 2009, Sorrento, Italy; 2009.

[30] Ma B, Ren J, Deng J, Yuan W. Flexible thermal sensor array on PI film substrate for underwater applications. In: Technical Digest IEEE Micro Electro Mechanical Systems Conference. J anuary 2010, Hong Kong; 2010.

[31] Li C, Wu P-M, Jung W, Ahn C. H, Shutter L. A, Narayan R. K. A novel lab-on-a-tube for multimodal monitoring of patients with traumatic brain injury. In: Technical digest of The 15th International Conference on Solid-State Sensors and Actuators. June 2009, Denver, USA; 2009.

[32] Naito J, Shikida M, Hirota M, Tan Z, Sato K. Miniaturization of on-wall in-tube flexible thermal flow sensor using heat shrinkable tube. In: Technical Digest IEEE Micro Electro Mechanical Systems Conference. January 2008, Tucson, USA; 2008.

[33] Yokota T, Naito J, Shikida M, Kawabe T, Hayashi Y, Sato K. Catheter type of flow sensor for trans-bronchial measurement for lung functions. Technical digest of The 15th International Conference on Solid-State Sensors and Actuators. June, 2009, Denver, USA; 2009.

[34] Shikida M, Naito J, Yokota T, Kawabe T, Hayashi Y, Sato K. A Catheter-type Flow Sensor for Measurement of Aspirated- and Inspired-air Characteristics in Bronchial Region. Journal of Micromechnics and Microengineering 2009;19(10) 105027

[35] King L. V. On the Convection of Heat from Small Cylinders in a Stream of Fluid: Determination of the Convection Constants of Small Platinum Wires with Applications to Hot-Wire Anemometry. Philosophical Transactions of the Royal Society of London. Series A, Containing Papers of a Mathematical or Physical Character 1914;90(622) 563-570.

[36] Tan Z, Shikida M, Hirota M, Sato K, Iwasaki T, Iriye Y. Experimental and theoretical study of an on-wall in-tube flexible thermal sensor. Journal of Micromechnics and Microengineering 2007;17(4) 679-686.

[37] Tan Z, Shikida M, Hirota M, Xing Y, Sato K, Iwasaki T, Iriye Y. Characteristics of on-wall in-tube thermal flow sensor under radially asymmetric flow condition. Sensors and Actuators A 2007;138(1) 87-96.

[38] Yoshikawa K, Iwai S, Shikida M, Sato K. Attached-type flexible flow sensor for air conditioning network. Technical digest of The 16th International Conference on Solid-State Sensors and Actuators. June 2011, Beijing, China; 2011.

[39] Shikida M, Yokota T, Kawabe T, Funaki T, Matsushima M, Iwai S, Matsunaga N, Sato K. Characteristics of an optomized catheter-type thermal flow sensor for measuring reciprocating airflows in bronchial pathways. Journal of Micromechnics and Microengineering 2010;20(12) 125030.

[40] Shikida M, Yokota T, Naito J, Sato K. Fabrication of a stent-type thermal flow sensor for measuring nasal respiration. Journal of Micromechnics and Microengineering 2010;20(5) 055029.

IntechOpen

Chapter 19

Single Cell Nanosurgery System

Toshio Fukuda, Masahiro Nakajima,
Yajing Shen and Masaru Kojima

1. Introduction

A model organism is one of the species that is extensively studied to understand particular biological phenomena, with the expectation that discoveries made in the organism model will provide insight into the workings of other organisms [1]. In particular, model organisms are widely used to explore potential causes and treatments for human disease when human experimentation would be unfeasible or unethical [2]. It shows some of the model organisms that have been used in a biomedical research.

The first and foremost consideration in the selection of any model organisms before conducting any bio-related research is how relevance the selected model organisms to human. If the first consideration is justified, then the second consideration which needs to be addressed is how practical and easy the selected model organisms for experimental endeavors.

Yeast is one of the simplest eukaryotic organisms (organism whose cells contain a clear defining membrane-bound structure of nucleus) but many essential cellular processes are conserved between yeast and humans. There are genes in yeast and mammals that encode very similar proteins [3]. Comparison of the yeast and human genomes, reported in 1997, revealed that 30% of known genes involved in human disease have yeast orthologs (i.e. functional homologs) [4]. Furthermore, hundreds of yeast genes exhibit a link to human disease genes as reported by [5].

Yeast is a good experimental tool for molecular and cellular biology studies. Yeast growth and division can be controlled efficiently and effectively by adjusting environmental conditions. Furthermore, yeast cells divide in a similar manner to human cells.

Because of these advantageous features, yeast has become the model organism of choice for medicine-related research. For example, studies with yeast have contributed greatly to our knowledge of the regulation of eukaryotic cell division, including the cancer-related distur-

INTECH
open science | open minds

bances [6]. Up to now, yeast has maintained its role as a useful model system in fundamental studies of disease processes.

2. Single cell nanosurgery system based on nanorobotic manipulation system

2.1. Single cell nanosurgery system

We have been proposed a "Nanolaboratory" based on nanorobotic manipulation system from around 2000 [7]. It is one of the systems to realize various nanoscale fabrication and assembly to develop novel nanodevices to integrate borderless technologies based on nanorobotic manipulation system. It is readily applied to the scientific exploration of macroscopic phenomena and the construction of prototype nanodevices. It would be one of the most significant enabling technologies to realize the manipulation and fabrication technology with individual atoms and molecules for the assembly of devices. Recently, the investigation of Nanoelectromechanical Systems (NEMS) has attracted much attention [8-11]. It is expected to realize high integrated, miniaturized, and multi-functional devices for various applications. One of the effective ways is the direct usage of the bottom-up fabricated nanostructures.

Nanolaboratory can be applied for the single cell analysis and manipulations. As show in Figure 1, the integration is important for the single cell nanosurgery system between micro and nanorobotic manipulators under various microscopes. The applications under dry, semi wet, and wet conditions can be done under TEM/SEM, E-SEM and optical microscope (OM). The nanomanipulation system inside TEM/SEM is a fundamental technology for property characterization of nano materials, structures and mechanisms, with the fabrication of nano building blocks, and for the assembly of nano devices. The nanomanipulation system inside E-SEM provides single cell manipulation and analysis under nano-scale high resolution images for the application of nanodevices or nanotools assembled under dry condition. OM micromanipulation system is used under water, hence the biological cells can be cultured with medium.

2.2. Nanorobotic manipulations

Nanorobotic manipulation; nanomanipulation, has been received much more attention, because it is an effective strategy for the property characterizations of individual nano-scale materials and the construction of nano-scale devices [12]. They might finally be the core-most part of nanotechnology. One of the attractive future applications of nanomanipulation is to realize the ultimate goal of nanotechnology, or nanomanipulation, is considered.

To manipulate nano-scale objects, it is needed to observe them with a resolution higher than nano-scale. Hence, the manipulators and observation systems, microscopes in general, are necessary for nanomanipulations. Figure 1 shows the strategies of nanomanipulations with various kinds of microscopes. The nanomanipulation under various microscopes for 2D/3D nanomanipulations. Optical microscope (OM) is one of the most historical and basic micro-

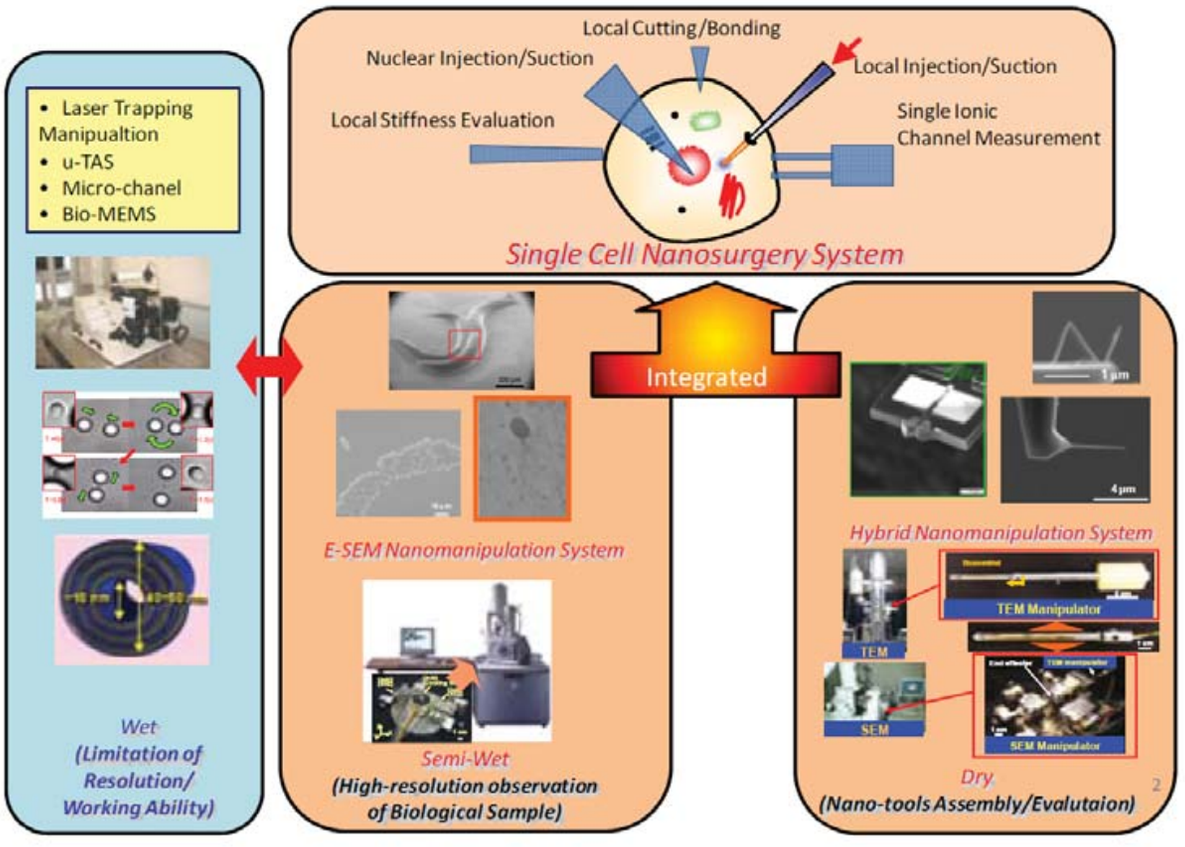

Figure 1. Single cell nanosurgery system based on micro/nanomanipulators under various microscopes (wet/semi-wet/dry conditions).

scope. However, its resolution is limited to ~100 nm because of the diffraction limit of optical wavelength (~400 - ~800 nm) explained by the well-known Abbe's law [13].

The scanning tunnelling microscopes (STMs) or atomic force microscopes (AFMs), have functions of both observation and manipulation in nano-scale. Their high resolution makes them capable of atomic manipulation. In 1990, Eigler and Schweize demonstrated that the first atom practice nanomanipulation with scanning tunnelling microscope (STM) [14]. Avouris et al. applied an AFM to bend and translate carbon nanotubes (CNTs) on a substrate [15]. They combined the techniques with an inverse process, namely straightening, by pushing along a bent tube, and realized the translation of a tube to another place. Ning Xi et. al at Michigan State University, developed AFM based nanomanipulation system with interactive operation system [16, 17]. The system realized a real-time visual feedback during AFM based nanomanipulation.

Normally, SPM systems have limit for the observation in 2D plane with quite smooth surface. Moreover, the observation area is limited and long time is needed to get one image (more than mins). This limitation rises up as 3D nanomanipulation of nanostructures. On the other hand, the electron microscopes (EMs) provide atomic scale resolution with the electron beam which wave length is less than ~0.1 Å. EMs are divided mainly two types as scanning electron

microscopes (SEMs) and transmission electron microscopes (TEMs). For example, M. F. Yu et. al presented the tensile strength of individual CNTs inside a SEM [18]. However the resolution of SEM, generally ~1 nm resolution, is approximately one order in magnitude lower than that of a TEM. High resolution and transmission image of TEMs are useful for measurement and evaluation of nano-scale objects. Kizuka et.al proposed the manipulation holder inside high-resolution transmission electron microscope (HR-TEM). The manipulator was specially designed with atomic level positioning resolution [19].

However, the specimen chamber and observation area of TEM are too narrow to contain manipulators with complex functions. Hence, special sample preparation techniques are also needed. We proposed a hybrid nanorobotic manipulation system which is integrated TEM and SEM nanorobotic manipulators as core system for the Nanolaboratory [20, 21]. The strategy is named as hybrid nanomanipulation so as to differentiate it from those with only an exchange-able specimen holder. The most important feature of the manipulator is that it contains several passive DOFs, which makes it possible to perform relatively complex manipulations whereas to keep compact volume to be installed inside the narrow vacuum chamber of a TEM [22].

Recently single cells analysis has been much more attentions because of the progress of the micro/nano scale techniques on the local environmental measurements and controls [23]. Under conventional SEMs and TEMs, the sample chambers of these electron microscopes are set under the high vacuum (HV) to reduce the disturbance of electron beam for observation. To observe water-containing samples, for example bio-cells, the appropriate drying and dying treatments are needed before observations. Hence, direct observations of water-containing samples are normally quite difficult through these electron microscopes.

On the other hand, the environmental-SEM (E-SEM) can be realized the direct observation of water-containing samples with nanometer high resolution by specially built secondly electron detector [24]. The evaporation of water is controlled by the sample temperature (~0 - ~40 °C) and sample chamber pressure (10 - 2600 Pa). The unique characteristic of the E-SEM is the direct observation of the hydroscopic samples with non-drying treatment. Hence, the nano-manipulation inside the E-SEM is considered to be an effective tool for a water-containing sample with nanometer resolution [25-28].

3. Single cell analysis based on an E-SEM nanorobotic manipulation system

Single cells analysis needs to be investigated through the micro/nano scale techniques based on the local environmental measurements and controls. We developed the Environmental-SEM (E-SEM) nanorobotic manipulation system to manipulate and control the local environ-ments for biological samples in nano scale (Figure 2). It realized that direct observation and manipulation of water-containing biological samples under nanometer high resolution imaging.

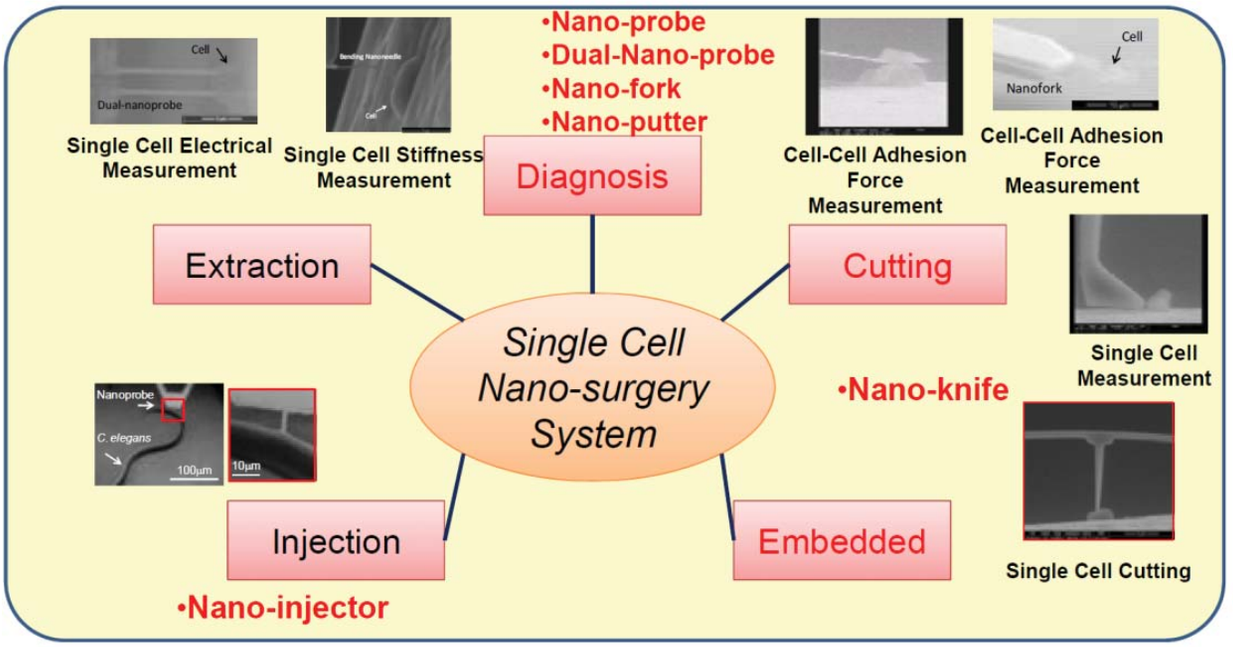

Figure 2. Single Cell Nano-surgery System with various nano-tools

In this chapter, the novel local stiffness evaluation, local cutting, and local extraction of biological organism are presented by micro-nanoprobes based on the E-SEM nanorobotic manipulation system for future cell diagnosis and surgery system.

3.1. Adhesion force measurement of single cell using nano-putter

Cell activities, such as embryogenesis, mitosis, morphogenesis, cell orientation, cell motility, and survival depend on attachment to neighboring cells and the extracellular matrix. Cellular attachment to extracellular matrices influences cell morphology, cell function, and signaling mechanisms that direct cellular proliferation and differentiation [29]. Cell-surface interaction is important in the development of any material or device for biomedical applications, since the performance of a medical device in the body must be compatible with the surrounding tissue [30, 31]. Understanding of the cell adhesion process would benefit the development of suitable biomaterials or device for both tissue engineering and medical fields.

Cell adhesion processes are influenced by numerous parameters, such as the nature of the biomaterial and its surface characteristics (roughness, topography, chemical composition, surface wettability, surface charge and surface treatments) have been investigated. However, the effect of ambient humidity on cell adhesion has had less attention, especially at the single cell level. Understanding the adhesion force at various humidity conditions could help us to better understand the processes of cell-directed integration during water evaporation. The understanding is also useful in controlling yeast infections at wet environment. Moreover, cell adhesion is influenced by the surface energy of substrate strongly, but the mechanism is still not clear [32]. The study of cell adhesion on substrates with different surface energy could help us to understand the adhesion mechanism better.

We presented a yeast cell adhesion force measurement performed using the nanorobotic manipulation system inside the ESEM [33, 34, 35]. Figure 3 (A) shows a typical force-displacement curve during the single cell adhesion force measurement. Figure 3 (B) shows the initial position of the micro putter and the single cell. The micro putter was driven by the nanorobotic manipulation system. First, it was moved towards the cell until it contacted the cell (Figure 3 (C)). Then, a continuous movement was applied to the micro putter by the nanomanipulator. The micro putter beam deflected owing to the increasing pushing force. Figure 3 (D) shows the deflection of the micro putter during the adhesion force measurement. Finally, the cell was detached from its initial position under a certain force (Figure 3 (E)). The maximum force during this manipulation procedure was defined as the adhesion force.

Single yeast cell adhesion force measurement was performed at three humidity conditions, i.e. 100%, 70% and 40%. The mean adhesion force and the deviation are with 95% confidence at each humidity conditions. It demonstrates that the yeast cell adhesion forces range from 10 to 25 μN at various humidity conditions. The adhesion forces were 11.0 ± 5.1 μN, 17.4 ± 4.7 μN and 23.5 ± 6.1 μN at 100%, 70% and 40% relative humidity conditions respectively. It showed clearly that the cell adhesion was affected by the ambient humidity. The cell adhesion force is larger at low humidity than at high humidity. For example, the cell adhesion force was 23.5 μN at a humidity of 40%, which was 1.14 times larger than the force 11.0 μN at humidity 100%.

3.2. Single cell cutting using nano-knife

Cell cutting is an important step in cell analysis processes. For instance, it was widely used to prepare cell specimen slices for the observation of an inner structure [36]. Different to group cells analysis, research on individual cells could give accurate data rather than average results. Single cell analysis can help us to understand the biological processes more accurately. In-situ single cell cutting technique could potentially benefit cell analysis, such as single cell operation and disease treatment.

Recently, a nano knife fabricated from a carbon nanotube (CNT) has been developed for the purpose of cell cutting [37]. The nano knife was designed by welding a CNT across two tungsten needles inside a scanning electron microscopy (SEM). This device can reduce the angle by which the sample is bent during cutting, due to the small diameter of the CNT. It can be seen clearly that the nano knife can leave a mark on the epon resin surface, which means it can cut very thin slices of cells. However, the bonding force between the CNT and tungsten probes by using electron beam induced deposition (EBID) method is quite small. There are still certain types of hard specimens such as bone, plants, and thick-walled spores. The CNT based nano knife may not be able to deal with such samples, since a larger cutting force is required, especially when the sample size is large.

We presented a nano knife with a buffering beam was designed for an in-situ single cell cutting purpose [38]. A schematic drawing of the single cell cutting using a nano knife is shown in Figure 4. The nano knife was immobilized to the nanomanipulator by using the electrical conductive tape inside the ESEM chamber. Under the driving of the nanorobotic manipulation system, the nano knife can move towards and cut the single cell finally. The cutting force can be calculated based on the deformation of the nanokinfe's beam.

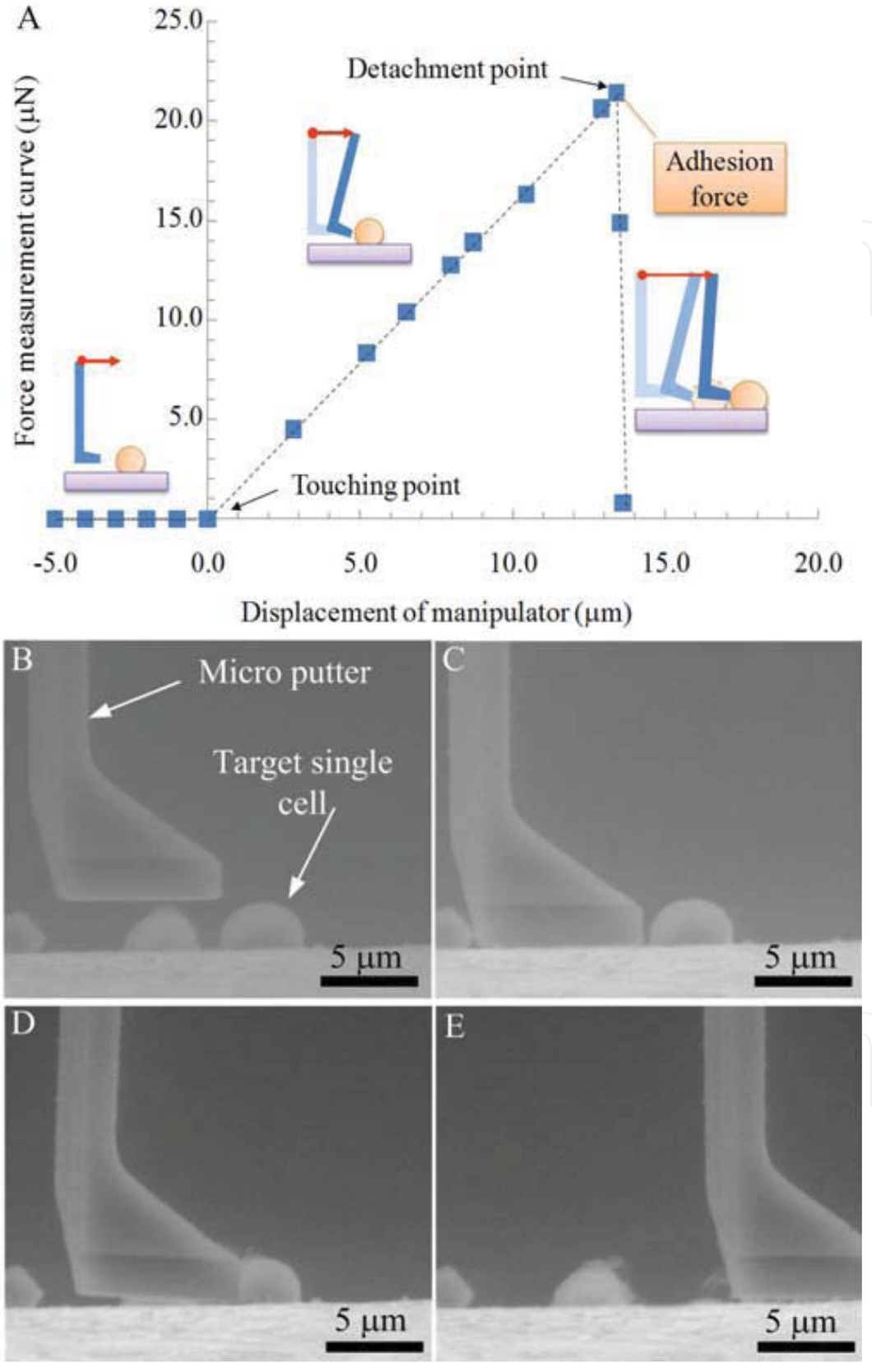

Figure 3. Single cell adhesion force measurement using micro putter inside ESEM.

The in situ single cell cutting experiment was performed using these three nano knives. Figure 5(A) shows the initial position of the nano knife and a single cell. Figure 5(B) shows the touching between the nano knife tip and the single cell. The deformation of the nano knife beam and the single cell during the cutting is shown in Figure 5(C). The deformation of the beam can be measured from the ESEM image directly using image analysis software. Therefore, the cutting force can be calculated based on Hooke's law. The separated single cell after cutting is shown in Figure 5(D). The sample slice angle can be measured from the ESEM image directly as well. Figure 5(E) shows the single cell cutting image using the 25° knife. Figure 5(F) shows the sample slice angle after cutting. The images of single cell cutting and sample slice angle after cutting using 45° knife are shown in Figure 5 (G) and Figure 5 (H).

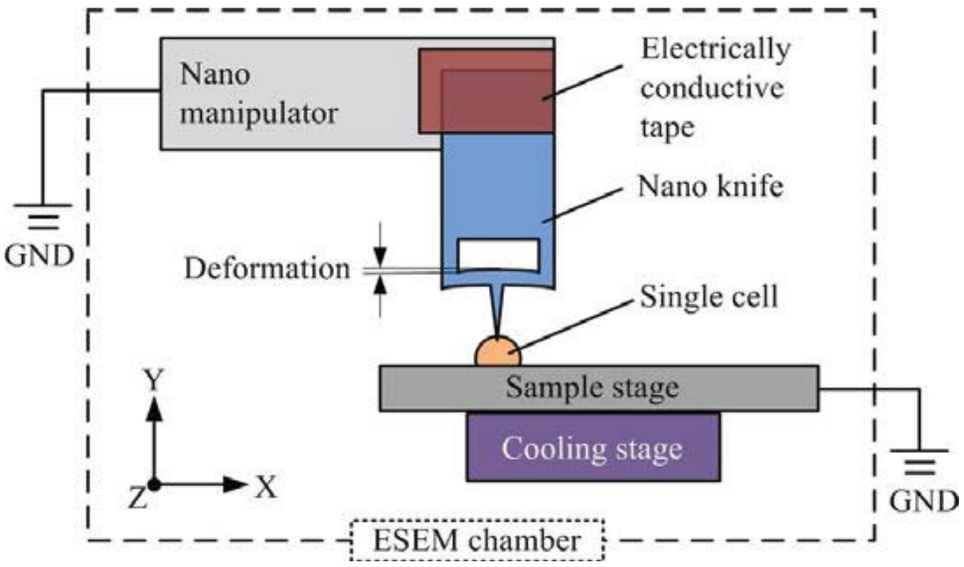

Figure 4. Schematic drawing of the single cell cutting experiment using nano knife inside ESEM.

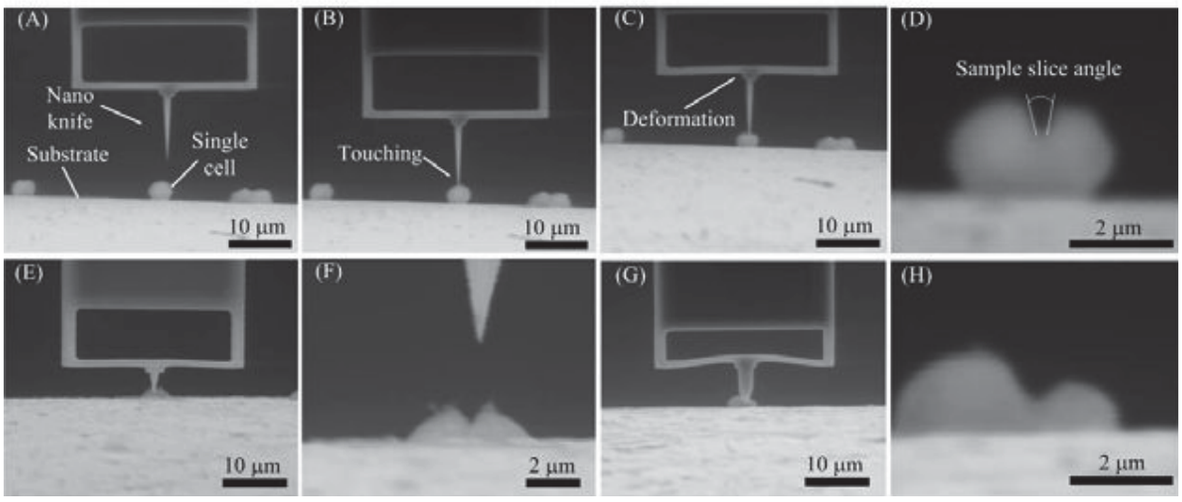

Figure 5. Single cell cutting using nano knife inside ESEM.

4. Conclusion

This chapter presents the single cell nanosurgery system based on nanomanipulation techniques. The micro-nano tools have been proposed to investigate single cell analysis to manipulate and control the local environment in micro-nano scale. The E-SEM nanomanipulation system was constructed to realize the local stiffness evaluation, local cutting, and local extraction of biological organism in nano-meter scale. The adhesion force measurement was presented by micro-putter for single cells. The single cell cutting was also described using nano-knife. As future direction, the multiple micro-nanotools are used continuously depending on the purposes by exchanging machinery system (NTExS: Nanotool Exchanger System) [39]. We are investigating on the nanoinjection applications for the Caenorhabditis elegans (C. elegans) as one of the model organisms [40, 41]

Acknowledgements

The authors are grateful to Prof. T. Inada N. Uozumi for providing with W303 yeast cells. This work was partially supported by a Grant-in-Aid for Scientific Research from the Ministry of Education, Culture, Sports, Science and Technology of Japan.

Author details

Toshio Fukuda, Masahiro Nakajima, Yajing Shen and Masaru Kojima

Department of Micro-Nano Systems Engineering, Nagoya University, Nagoya, Japan

References

[1] Fields S, Johnston M. Cell biology: Whither model organism research? Science 2005;307 1885 - 1886.

[2] Fox M. A. The case for animal experimentation: An evolutionary and ethical perspective: University of California Press; 1986.

[3] Botstein D, Chervitz S. A, Cherry J. M. Yeast as a model organism. Science 1997;277 1259 - 1260.

[4] Foury F. Human genetic diseases ? a cross-talk between man and yeast. Gene 1997;195 1-10.

[5] Mager W. H, Winderickx J. Yeast as a model for medical and medicinal research. TRENDS in Pharmacological Sciences 2005;26 265-273.

[6] Hartwell L. H. Yeast and cancer," Bioscience Reports 2002;22 373-394.

[7] Dong L. X, Arai F, Fukuda T. Destructive Constructions of Nanostructures with Carbon Nanotubes Through Nanorobotic Manipulation. IEEE Transaction on Mechatronics 2004;9 350-357.

[8] Siegel R. W, Hu E, Roco M. C. Nanostructure Science and Technology. Kluwer Academic Publishers; 1999.

[9] Craighead H. G. Nanoelectromechanical Systems. Science 2000; 290 1532-1535.

[10] Staples M, Daniel K, Sima M. J, Langer R. Applications of Micro- and Nano-Electromechanical Devices to Drug Delivery. Pharnaceutical Research 2006;23 847-863.

[11] Leary S. P, Liu C. Y, Apuzzo M. L. J. Toward the Emergence of Nanoneurosurgery: Part III - Nanomedicine: Targeted Nanotherapy, Nanosurgery, and Progress Toward the Realization of Nanoneurosurgery. Neurosurgery 2006;58 1009-1026.

[12] Du E, Cui H, Zhu Z. Review of Nanomanipulators for Nanomanufacturing. International Journal of Nanomanufacturing 2006;1 83-104.

[13] Hell S. W. Far-Field Optical Nanoscopy. Science 2007;316 1153-1158.

[14] Eigler D. M, Schweizer E. K. Positioning Single Atoms with a Scanning Electron Microscope. Nature 1990;344 524-526.

[15] Hertel T, Martel R, Avouris P. Manipulation of Individual Carbon Nanotubes and their Interaction with Surfaces. The Journal of Physical Chemistry B 1998;102 910-915.

[16] Li G, Xi N, Chen H, Poneroy C, Prokos M. Videolized Atomic Force Microscopy for Interactive Nanomanipulation and Nanoassembly. IEEE Transaction on Nanotech 2005;4 605-615.

[17] Li G, Xi N, Yu M, Fung W-K. Development of Augmented Reality System for AFM based Nanomanipualiton. IEEE Transaction on Mechatronics 2004;9 358-365.

[18] Yu M. F, Lourie O, Dyer M. J, Moloni K, Kelley T. F, Ruoff R. S. Strength and Breaking Mechanism of Multiwalled Carbon Nanotubes under Tensile Load. Science 2000;287 637-640.

[19] Kizuka T, Yamada K, Deguchi S, Naruse M, Tanaka N. Cross-sectional Time Resolved High-Resolution Transmission Electron Microscopy of Atomic-Scale Contact and Noncontact-Type Scannings on Gold Surfaces. Physical Review B 1997;55 7398-7401.

[20] Nakajima M, Arai F, Fukuda T. In situ Fabrication and Electric Actuation of Telescoping Nanotube inside TEM through Hybrid Nanorobotic Manipulation System. In: Proceedings of the 2006 IEEE/RSJ International Conference on Intelligent Robotics and Systems (IROS 2006); 2006., 1915-1920.

[21] Nakajima M, Arai F, Fukuda T. In situ Measurement of Young's Modulus of Carbon Nanotube inside TEM through Hybrid Nanorobotic Manipulation System. IEEE Transsaction on Nanotechnology 2006;5 243-248.

[22] Leary S. P, Liu C. Y, Apuzzo M. L. J. Toward the Emergence of Nanoneurosurgery. Neurosurgery 2006;58 1009-1026.

[23] Donald A. M. The use of environmental scanning electron microscopy for imaging wet and insulating materials. Nature Materials 2003;2 511-516.

[24] Nakajima M, Arai F, Fukuda T. Nanofixation with Low Melting Metal Based on Nanorobotic Manipulation. Proceedings of the 6th IEEE International Conference on Nanotechnology (IEEE-Nano 2006)., 925-928.

[25] Ahmad M. R, Nakajima M, Kojima S, Homma M, Fukuda T. The effects of cell sizes, environmental conditions and growth phases on the strength of individual w303 yeast cells inside esem. IEEE Transactions on Nanobioscience 2008;7 185-193.

[26] Ahmad M. R, Nakajima M, Kojima S, Homma M, Fukuda T. In-situ Single Cell Mechanics Characterization of Yeast Cells using Nanoneedles inside Environmental-SEM. IEEE Transactions on Nanotechnology 2008;7(5) 607-616.

[27] Ahmad M. R, Nakajima M, Kojima S, Homma M, Fukuda T. Nanoindentation Methods to Measure Viscoelastic Properties of Single Cells using Sharp, Flat and Buckling Tips inside ESEM. IEEE Transactions on Nanobioscience 2010;9(1) 12-23.

[28] Ahmad M. R, Nakajima M, Kojima S, Homma M, Fukuda T. Buckling Nanoneedle for Characterizing Single Cells Mechanics inside Environmental SEM. IEEE Transactions on Nanotechnology 2011;10(2) 226-236.

[29] Gumbiner B. M. Cell adhesion: the molecular basis of tissue architecture and morphogenesis. Cell 1996., 84 345.

[30] Lelievre S, Weaver V. M, Bissell M. J. Extracellular matrix signaling from the cellular membrane skeleton to the nuclear skeleton: a model of gene regulation. Recent Progress in Hormone Research (1996)., 51 417.

[31] Hong-Geller E. A role for cell adhesion in beryllium-mediated lung disease. Journal of Occupational and Environmental Hygiene 2009;6 727-731.

[32] Marcotte L, Tabrizian M. Sensing surfaces: Challenges in studying the cell adhesion process and the cell adhesion forces on biomaterials. Irbm 2008;29 77-88.

[33] Shen, Y, Nakajima, M, Kojima, S, Homma, M, Kojima, M, & Fukuda, T., Single cell adhesion force measurement for cell viability identification by using AFM cantilever based micro putter., Measurement science and technology, (2011), 22(11) 115802

[34] Shen, Y, Ridzuan, M, Nakajima, M, Kojima, S, Homma, M, & Fukuda, T., Evaluation of the single yeast cell's adhesion to ITO substrates with various surface energies via

ESEM nanorobotic manipulation system. IEEE Transactions on Nanobioscience, (2011)., 10(4), 217-224.

[35] Shen, Y, Nakajima, M, Ridzuan, M, Kojima, S, Homma, M, & Fukuda, T. Effect of ambient humidity on the strength of the adhesion force of single yeast cell inside environmental-SEM. Ultramicroscopy (2011). , 111(8), 1176-1183.

[36] Mobius, W. Cryopreparation of biological specimens for immunoelectron microscopy. Annals of Anatomy-Anatomischer Anzeiger (2009)., 191-231.

[37] Singh, G, Rice, P, Mahajan, R, & Mcintosh, J. Fabrication and characterization of a carbon nanotube-based nanoknife. Nanotechnology (2009). 20 (9), 095701.

[38] Shen, Y, Nakajima, M, Yang, Z, Kojima, S, Homma, M, & Fukuda, T. Design and characterization of nanoknife with buffering beam for in situ single cell cutting. Nanotechnology (2011), 22 (30), 305701.

[39] Nakajima, M, Kawamoto, T, Hirano T, Kojima, M. & Fukuda, T. Nanotool Exchanger System based on E-SEM Nanorobotic Manipulation System. Proceedings of the 2012 IEEE International Conference on Robotics and Automation (ICRA 2012), (2012), 2773-2778.

[40] Nakajima, M, Hirano, T, Kojima, M, Hisamoto, N, Homma, M, & Fukuda, T. Direct Nano-injection Method by Nanoprobe Insertion based on E-SEM Nanorobotic Manipulation under Hybrid Microscope. Proceedings of the 2011 IEEE International Conference on Robotics and Automation (ICRA 2011), (2011), 4139-4144.

[41] Nakajima, M, Hirano, T, Kojima, M, Hisamoto, N, Nakanishi, N, Tajima, H, Homma, M, & Fukuda T. Local Nano-injection of Fluorescent Nano-beads inside C. elegans based on Nanomanipulation. Proceedings of the 2012 IEEE/RSJ International Conference on Intelligent Robotics and Systems (IROS 2012) (2012), 3241-3246.